

Large N Master Field Optimization: the Quantum Mechanics of two Yang-Mills coupled Matrices

Kagiso Mathaba*, Mbavhalelo Mulokwe[†] and João P. Rodrigues[‡]

National Institute for Theoretical and Computational Sciences
 School of Physics and Mandelstam Institute for Theoretical Physics
 University of the Witwatersrand, Johannesburg
 Wits 2050, South Africa

Abstract

We study the large N dynamics of two massless Yang-Mills coupled matrix quantum mechanics, by minimization of a loop truncated Jevicki-Sakita effective collective field Hamiltonian. The loop space constraints are handled by the use of master variables. The method is successfully applied directly in the massless limit for a range of values of the Yang-Mills coupling constant, and the scaling behaviour of different physical quantities derived from their dimensions are obtained with a high level of precision. We consider both planar properties of the theory, such as the large N ground state energy and multi-matrix correlator expectation values, and also the spectrum of the theory. For the spectrum, we establish that the $U(N)$ traced fundamental constituents remain massless and decoupled from other states, and that bound states develop well defined mass gaps, with the mass of the two degenerate lowest lying bound states being determined with a particularly high degree of accuracy. In order to confirm, numerically, the physical interpretation of the spectrum properties of the $U(N)$ traced constituents, we add masses to the system and show that, indeed, the $U(N)$ traced fundamental constituents retain their "bare masses". For this system, we draw comparisons with planar results available in the literature.

1 Introduction

Multi-matrix systems ¹ are important in many different physical settings, not only as of finite sized matrices, but particularly in their large N limit [1]. They are expected to provide a reduced ansatz for large N gauge theories, both in

*Email: kgs.mathaba@gmail.com

[†]Email: mbavhalelo.mulokwe@wits.ac.za

[‡]Email: joao.rodrigues@wits.ac.za

¹We have in mind the path integral or the quantum mechanics of a finite number of matrices.

the path integral [2, 3, 4, 5, 6] and Hamiltonian formulations [7, 8], and both for unitary as well as hermitian matrices. Their interpretation as $D0$ branes [9] has led to the suggestion that they may provide a definition of M theory [10], also argued to be valid for the path integral [11]. The AdS/CFT correspondence [12, 13, 14] has highlighted the importance of $\mathcal{N} = 4$ SYM theory, with its bosonic adjoint scalar sector, and ensuing integrability properties [15] and Hamiltonian reductions [16], [17, 18, 19]. They are used in the study of black holes [20, 21, 22]².

We study in this communication the large N properties of the Hamiltonian of two massless matrices interacting via a Yang-Mills potential. We are able to study the system directly in the large N limit and directly in the massless limit. In general [23, 24], properties of the massless system are obtained by extrapolation of a system with a finite mass parameter to zero. In our case, being able to work directly with the massless system, we are able to obtain the asymptotic scaling behaviour of physical quantities and correlators, and determine their parameters, with a high degree of accuracy.

In addition to its interpretation as a reduced model, $D0$ or bosonic scalar subsector of $\mathcal{N} = 4$ SYM, this Hamiltonian has associated with it a number of puzzles, mainly around the properties of its spectrum and of the presence or not of a mass gap [25, 26, 27]. Within the context of the $1/N$ expansion, we provide a definite answer to this question in this article.

Our approach is based on the collective field theory Hamiltonian of Jevicki and Sakita [28]. This Hamiltonian is an exact re-writing of a given theory in terms of its (gauge) invariant variables. The large N (planar) background is then obtained semiclassically as the minimum of an effective potential V_{eff} and, when expanded about this large N background, the collective field theory Hamiltonian generates $1/N$ corrections systematically³.

The idea behind the method is to implement a change of variables from the original variables of the theory, generically denoted by $X_{\mathcal{A}}$, to the invariant set of operators (the collective fields), generically denoted by $\phi(C)$, and to require explicit hermiticity of the collective field Hamiltonian. This change of variable is accompanied by a Jacobian J . In general J is not known explicitly, but it satisfies the following equation

$$\sum_{C'} \frac{\partial \ln J}{\partial \phi^\dagger(C')} \Omega(C', C) = w(C) - \sum_{C'} \frac{\partial \Omega(C', C)}{\partial \phi^\dagger(C')}.$$

This is sufficient to obtain explicitly the collective field Hamiltonian in terms of $\phi(C)$ and its canonical conjugate $\pi(C)$. In general,

$$\Omega(C, C') = \sum_{\mathcal{A}} \frac{\partial \phi^\dagger(C)}{\partial X_{\mathcal{A}}^\dagger} \frac{\partial \phi(C')}{\partial X_{\mathcal{A}}}, \quad w(C) = \sum_{\mathcal{A}} \frac{\partial^2 \phi(C)}{\partial X_{\mathcal{A}}^\dagger \partial X_{\mathcal{A}}}.$$

$\Omega(C, C')$ joins two loops into a sum of single loops⁴, and $w(C)$ splits a given

²There is a vast literature on matrix models; we have tried to highlight only some key developments in their application, with emphasis on YM coupled systems.

³For a single matrix based example, see for instance [29], [30]. Also, although we consider matrix valued systems in this communication, the same is true of vector valued field theories.

⁴The terminology "loop" is inherited from gauge theories, where the gauge invariant variables are Wilson loops. But in this communication they refer to operators that are invariant under the gauge symmetries allowed by the system under consideration.

loop into a sum of two (in general smaller) loops. Details of their form will be given in the following.

The collective field Hamiltonian H_{col} is ideally suited to a numerical approach based on minimisation of the effective potential V_{eff} , in a truncated loop space $H_{col} \rightarrow H_{col}^{trunc}$ that can be systematically increased and ascertained for convergence and accuracy. Indeed, already some time ago [31, 32], this approach was successfully implemented in the context of $2 + 1$ lattice gauge theories with Wilson's one-plaquette action [33]. Systems of unitary matrices have a phase transition between a strong and weak phase, and it was established in [31, 32] that in the weak coupling phase the minimization has to be accompanied by a constraint:

$$\begin{cases} \text{Minimize } V_{eff}^{trunc}, \\ \Omega(C, C') \succeq 0. \end{cases} \quad (1)$$

In other words, the large N expectation values of the loop variables $\phi(C)$ must satisfy the constraint that the matrix $\Omega(C, C')$ is semi-positive definite, with a number of eigenvalues saturating to zero in the weak coupling regime. This was shown to also be the case when considering loop equations [34].

This constraint is not difficult to understand: the large N limit of the single unitary matrix integral has a well known third order phase transition [35], described in terms of the density of its (phases of) eigenvalues $\rho(\theta)$ as:

$$\left\{ \begin{array}{l} \rho(\theta) = \frac{1}{2\pi} (1 + \frac{2}{\lambda} \cos \theta), \quad -\pi \leq \theta \leq \pi \quad \text{for } \lambda \geq 2, \\ \left\{ \begin{array}{l} \rho(\theta) = \frac{2}{\pi\lambda} \cos \frac{\theta}{2} \sqrt{\frac{\lambda}{2} - \sin^2 \frac{\theta}{2}}, \quad |\theta| < 2 \sin^{-1} \sqrt{\frac{\lambda}{2}} \\ \rho(\theta) = 0, \quad 2 \sin^{-1} \sqrt{\frac{\lambda}{2}} \leq |\theta| \leq \pi \end{array} \right. \quad \text{for } \lambda \leq 2. \end{array} \right. \quad (2)$$

In the strong coupling regime, the density of eigenvalues is periodic with period 2π . For weak coupling, the density of eigenvalues develops finite support within the interval $[-\pi, \pi]$, and $\rho(\theta) = 0$ outside this finite support.

A similar phase transition and pattern in the density of eigenvalues is present in the large N limit of the quantum mechanics of single unitary matrix systems [36, 37, 38, 39]. Systems of hermitian matrices have only one single (weak) phase, so ensuring that $\phi(x) = 0$ outside their finite support in order that the density of states remains non-negative is of paramount importance.

For a single hermitian $N \times N$ matrix M , with invariants $\phi_k = \text{Tr}(e^{-ikM}) = \sum_{i=1}^N e^{-ik\lambda_i}$, the density of eigenvalues is simply its Fourier transform, $\phi(x) = \int dk/2\pi e^{ikx} \phi_k = \sum_{i=1}^N \delta(x - \lambda_i)$. Then:

$$\Omega(k, k') = kk' \phi_{k'-k}, \quad \Omega(x, y) = \partial_x \partial_y (\phi(x) \delta(x - y)).$$

So, in this simple case, $\Omega(x, y)$ is seen to have zero eigenvalues when the density matrix $\langle x | \hat{\phi} | y \rangle = \phi(x) \delta(x - y)$ has zero eigenvalues, or when $\phi(x) = 0$. For single matrix systems then, this constraint on Ω is easily related to the requirement that the density is non-negative.

In the case of more complex multi-matrix systems, and in the context of the collective field theory approach, the required constraint is then that the loop space matrix

$$\Omega(C, C') = \sum_{\mathcal{A}} \frac{\partial \phi^\dagger(C)}{\partial X_{\mathcal{A}}^\dagger} \frac{\partial \phi(C')}{\partial X_{\mathcal{A}}} = \sum_{C''} y(C, C', C'') \phi(C'')$$

is semi-positive definite. This follows from the definition of $\Omega(C, C')$, on the left hand side of the above equation, but no longer apparent once $\Omega(C, C')$ is expressed in terms of loop variables, as on the right hand side of the above equation. The semi-positiveness condition results in a number of inequalities amongst the loop variables. These are the non-linear constraints that large N expectation values of invariant operators have to satisfy, some of which are saturated. For instance, if the $X_{\mathcal{A}}$'s are hermitian matrices, the operation $\frac{\partial}{\partial X_{\mathcal{A}}}$ acting on a single trace loop of a product of these matrices removes $X_{\mathcal{A}}$ everywhere where it is present along the loop and "opens up an open string". $\Omega(C, C')$ can then be thought of as a matrix of (linear combinations of) open string inner products, linking to the interpretation as suggested in [40].⁵

Interest in the development of numerical techniques applicable directly to the large N limit properties of multi matrix systems has been rekindled recently [40, 41, 42, 43, 44], and the importance the loop space constraints re-discovered [40, 41, 42, 43], in a program generically referred to as numerical bootstrap. In [40, 43, 45] the constrained optimisation problem uses semidefinite programming in solving loop equations directly in loop space. In [41], the loop equations are iterated and a set of small loops adjusted to satisfy the constraints, and this method is generalized to matrix quantum mechanics in [42], where some exact bounds are also obtained.

In this article we carry out a numerical study of the large N limit of the quantum mechanics of two hermitian matrices coupled by a Yang-Mills potential using a truncated collective field Hamiltonian. We are able to carry out this study directly in the massless limit, with the different loop quantities considered exhibiting the expected scaling properties with an extremely high degree of accuracy. As indicated earlier, since the collective hamiltonian is an exact loop space re-writing of the large N theory, it has a systematic $1/N$ expansion. In particular then, and as a quantum mechanical system, we are able to study its mass spectrum in addition to the planar properties of the theory. The study of the spectrum and ensuing absence or presence of mass gaps is of particular importance to matrix gauge theories. We believe that currently, this is the only method able to provide information about the large N spectrum of the theory.

The issue of constraints is addressed by the use of "master variables" [32, 44, 46]. These are variables that satisfy the constraints explicitly, of which the original variables are an example. In addition to satisfying the constraints in the planar limit, they can be used to set up the spectrum equations of the theory [46]. For two matrix systems, we keep one of the matrices diagonal and the other as an arbitrary $N \times N$ hermitian, so that there are $N(N + 1)$ master variables.

The fact that another parameter N has been introduced in addition to the truncation parameter may seem undesirable. But the extensive study of two matrix hamiltonians with cubic, quartic and mixed quadratic potential carried in [44] as well as further evidence provided in this article establish the stability and accuracy of this approach⁶.

⁵For a unitary matrices, $\partial/\partial X_{ab} \rightarrow U_{bc}\partial/\partial U_{ab} (= -U_{ca}^\dagger/\partial U_{cb}^\dagger)$.

⁶It also opens the possibility of direct studies of stringy (gravity and brane) phenomena emerging from properties of single trace operators of length l related to different powers of N , as embedded in the AdS/CFT correspondence [12, 13, 14],[16],[48]. This is beyond the scope of this communication.

Loop equations of the $d = 0$ integral correspond to the statement of minimization of the large N loop collective effective potential of a suitably defined quantum mechanical Hamiltonian, namely the Fokker-Planck Hamiltonian [34]⁷. This is the best way to understand that constraints, (which in the collective field approach are encapsulated in the statement that $\Omega(C, C') \succeq 0$) arise even in the context of loop equations [34], and as argued differently and more recently in [40]. An extensive study of two matrix loop equations with cubic, quartic and mixed quadratic potential was carried in [44], which were shown to be satisfied to a very high level of accuracy. In this article, however, we are interested in the matrix quantum mechanics Hamiltonian of two Yang-Mills coupled matrices.

This article is organized as follows: after the current Introduction, Section 2 describes the method, the loop truncation and the use of master variables in dealing with the loop space constraints. Their use in obtaining both the large N loop background, and concomitant planar quantities, as well as the $1/N$ spectrum, is described. In Section 3 we apply the method to the large N limit of the quantum mechanics of two Yang-Mills coupled, massless matrices. We find that the method displays perfect stable convergence directly in this massless limit. Moreover, physical quantities exhibit the scaling behaviour determined by their dimensions with a very high level of accuracy, both for planar quantities and for the $1/N$ spectrum. In other words, the loop truncated collective field Hamiltonian is entirely consistent with the scaling properties of the full massless theory. Only correlators of zero charge of the $SO(2) \simeq U(1)$ symmetry of the system are shown to develop non-zero planar expectation values, and we assign charges to spectrum states. For the spectrum, we argue that the two lowest states, the $U(N)$ traced constituent single particle states⁸, are numerically massless, and associate them with the non-interacting $U(1) \times U(1)$ subgroup of the system. Higher energy (bound) states develop well defined mass-gaps. In order to confirm our physical interpretation of the two lowest degenerate states as massless states, we add masses to the system in Section 4, where it is verified indeed that their "bare mass" is not corrected. Mass corrected fits to the planar ground state energy, to the first few bound states and to planar correlators are presented, some of which are compared with (the few results available in) the literature. As for the massless case, it is confirmed that only zero charge correlators develop non-zero expectation values, and charges to spectrum states are assigned. Section 5 is left for a conclusion and future outlook. The Appendix discusses estimates of errors in our numerical method.

2 Method, loop truncation and master variables

We consider the quantum mechanics of two $N \times N$ hermitian matrices X_A , $A = 1, 2$, interacting via a Yang-Mills potential:

$$\hat{H} = \frac{1}{2} \sum_{A=1}^2 \text{Tr} P_A^2 + \frac{m^2}{2} \sum_{A=1}^2 \text{Tr} X_A^2 - \frac{g_{YM}^2}{N} \text{Tr} [X_1, X_2]^2 = \frac{1}{2} \sum_{A=1}^2 \text{Tr} P_A^2 + \text{Tr}(V(X_A)).$$

P_A is canonical conjugate to X_A , and m is a mass. The massless case $m = 0$ will be considered first in Section 3 and the massive case in Section 4. Note that

⁷This effective potential also gives the leading Large N loop configuration of the bosonic sector of supersymmetric multi matrix Marinari-Parisi [49] type models [50],[51].

⁸These are absent for $SU(N)$.

in terms of our conventions, 't Hooft's coupling λ is $\lambda = g_{YM}^2$.

The $U(N)$ invariant loops are single traces of products of the matrices X_A , up to cyclic permutations:

$$\phi(C) = \text{Tr}(\dots X_1^{m_1} X_2^{m_2} X_1^{n_1} X_2^{n_2} \dots).$$

For instance, with two matrices one has $[1\ 1] = \text{Tr}(X_1^2)$, $[1\ 2] = \text{Tr}(X_1 X_2)$, $[2\ 2] = \text{Tr}(X_2^2)$, with three matrices $[1\ 1\ 1] = \text{Tr}(X_1^3)$, $[1\ 1\ 2] = \text{Tr}(X_1^2 X_2)$, $[1\ 2\ 2] = \text{Tr}(X_1 X_2^2)$, $[2\ 2\ 2] = \text{Tr}(X_2^3)$, etc., with an obvious notation. We will continue to refer to the invariant variables as “loops”, for the historical reasons explained in the introduction.

The collective field Hamiltonian [28] in terms of the invariant loops $\phi(C)$ takes the form

$$H'_{col} = \frac{1}{2} \sum_{C, C'} \pi^\dagger(C) \Omega(C, C') \pi(C') + \frac{1}{8} \sum_{C, C'} w(C) \Omega^{-1}(C, C') w^\dagger(C') + V(\phi) + \Delta H',$$

where $\pi(C)$ is the canonical conjugate to $\phi(C)$, and

$$\begin{aligned} \Omega(C, C') &= \sum_{A=1}^2 \text{Tr} \left(\frac{\partial \phi^\dagger(C)}{\partial X_A^\dagger} \frac{\partial \phi(C')}{\partial X_A} \right) = \sum_{C''} y(C, C', C'') \phi(C'') \\ w(C) &= \sum_{A=1}^2 \text{Tr} \left(\frac{\partial^2 \phi(C)}{\partial X_A^\dagger \partial X_A} \right) = \sum_{C', C''} z(C, C', C'') \phi(C') \phi(C''). \end{aligned}$$

If C has length (number of matrices in the loop) $l(C)$ and C' has length $l(C')$, $\Omega(C, C')$ joins them into a number of loops of length $l(C) + l(C') - 2$. $w(C)$ splits the loop C of length $l(C)$ into sets of two loops C' and C'' with total lengths $l(C) - 2$. $\Delta H'$ contains subleading counterterms that need not be considered for the large N background and the spectrum.

We then consider

$$\begin{aligned} H_{col} &= \frac{1}{2} \sum_{C, C'} \pi^\dagger(C) \Omega(C, C') \pi(C') + V_{eff}(\phi), \\ V_{eff}(\phi) &\equiv \frac{1}{8} \sum_{C, C'} w(C) \Omega^{-1}(C, C') w^\dagger(C') + V(\phi). \end{aligned}$$

In order to exhibit explicitly the large N dependence, we let

$$\phi(C) \rightarrow \frac{\phi(C)}{N^{\frac{l(C)}{2}+1}} = \frac{\text{Tr}(\dots X_1^{m_1} X_2^{m_2} X_1^{n_1} X_2^{n_2} \dots)}{N^{\frac{l(C)}{2}+1}}, \quad \pi(C) \rightarrow N^{\frac{l(C)}{2}+1} \pi(C)$$

and obtain

$$H_{col} = \frac{1}{2N^2} \sum_{C, C'} \pi^\dagger(C) \Omega(C, C') \pi(C') + N^2 V_{eff}(\phi), \quad (3)$$

$$V_{eff}(\phi) \equiv \frac{1}{8} \sum_{C, C'} w(C) \Omega^{-1}(C, C') w^\dagger(C') + V(\phi). \quad (4)$$

It follows that the large N background is the minimum of V_{eff} subject to the constraint that $\Omega(C, C')$ is semi-positive definite.⁹

⁹The discussion next in this section follows closely that of [44], which is based on [31, 32, 46].

2.1 Truncation of loop space

For a given l ($l \geq 4$), Ω is truncated to be a $N_\Omega \times N_\Omega$ matrix, where N_Ω is the number of loops of length l or less. Ω itself, however, depends on loops with lengths up to $l_{\max} = 2l - 2$. If N_{loops} is the number of loops with length l_{\max} or less, then it is seen that V_{eff} in (4) is a function of N_{loops} :

$$V_{\text{eff}}^{\text{trunc}}(\phi(C), C = 1, \dots, N_{\text{loops}}) = \frac{1}{8} \sum_{C, C'=1}^{N_\Omega} w(C) \Omega^{-1}(C, C') w^\dagger(C') + V(\phi)$$

These parameters are listed in the following table for different levels of truncation.

l_{\max}	N_Ω	N_{loops}
4	9	15
6	15	37
8	23	93
10	37	261
12	57	801
14	93	2615
16	153	8923
18	261	31237

Table 1: Truncating loop space

2.2 Master fields and planar limit.

In order to minimize $V_{\text{eff}}^{\text{trunc}}$ subject to the constraint $\Omega(C, C') \succeq 0$, we introduce master variables ϕ_α that explicitly satisfy the constraint:

$$\Omega(C, C') = \sum_{\alpha} \frac{\partial \phi^\dagger(C)}{\partial \phi_\alpha} \frac{\partial \phi(C')}{\partial \phi_\alpha} \succeq 0$$

Specifically, we choose X_1 to be diagonal and X_2 an arbitrary $N \times N$ hermitian matrix. The master field then has $N^2 + N$ real components ϕ_α , $\alpha = 1, 2, \dots, N(N+1)$.

The planar limit is obtained by minimizing $V_{\text{eff}}^{\text{trunc}}$ with respect to the master variables. More precisely, at the minimum,

$$\frac{\partial V_{\text{eff}}^{\text{trunc}}}{\partial \phi_\alpha} \equiv \sum_{C=1}^{N_{\text{loops}}} \frac{\partial V_{\text{eff}}^{\text{trunc}}}{\partial \phi(C)} \frac{\partial \phi(C)}{\partial \phi_\alpha} \Big|_{\phi_\alpha^0} = 0, \quad \alpha = 1, 2, \dots, N(N+1) \quad (5)$$

$$\phi_{\text{planar}}(C) \equiv \phi(C) \Big|_{\phi_\alpha^0}, \quad C = 1, \dots, N_{\text{loops}}. \quad (6)$$

In general, $\partial V_{\text{eff}}^{\text{trunc}} / \partial \phi(C) \neq 0$. The planar background is specified by the large N expectation values $\phi_{\text{planar}}(C)$ of all gauge invariant operators.

Details of the numerical algorithm have been given in [44]. In this article, we have chosen a truncation with $l_{\max} = 14$, that is, 2615 N_{loops} and a $93 \times$

93 Ω matrix. For the master field, we took $N = 51$, corresponding to 2652 master variables. Evidence for the consistency of the truncation and stability with respect to different values of N has been provided in [44], and is also presented in Appendix A for the Yang-Mills coupled systems considered in this communication.

2.3 Spectrum and master variables

It is important to keep in mind that the $1/N$ expansion is an expansion in terms of loop variables. As such, letting

$$\phi(C) = \phi_{\text{planar}}(C) + \frac{1}{N}\eta(C), \quad \pi(C) = Np(C),$$

we expand (3) up to second order:

$$\begin{aligned} H_{\text{trunc}}^{(2)} &= N \sum_{C=1}^{N_{\text{loops}}} \frac{\partial V_{\text{eff}}^{\text{trunc}}}{\partial \phi(C)} \eta(C) + \frac{1}{2} \sum_{C, C'=1}^{N_{\text{loops}}} p^\dagger(C) \hat{\Omega}_0(C, C') p(C') \\ &+ \frac{1}{2} \sum_{C, C'=1}^{N_{\text{loops}}} \eta(C) V_0^{(2)}(C, C') \eta^\dagger(C'), \quad V_0^{(2)}(C, C') \equiv \left. \frac{\partial^2 V_{\text{eff}}^{\text{trunc}}}{\partial \phi(C) \partial \phi^\dagger(C')} \right|_{\phi_\alpha^0} \end{aligned}$$

But

$$\eta(C) = N \sum_{\alpha=1}^{N(N+1)} \left. \frac{\partial \phi(C)}{\partial \phi_\alpha} \right|_{\phi_\alpha^0} \delta \phi_\alpha$$

and hence the term linear in η in $H_{\text{trunc}}^{(2)}$ vanishes, as a result of (5).

It is important to note that $\hat{\Omega}_0$ is not the same as Ω_0 . Ω_0 is a $N_\Omega \times N_\Omega$ matrix (Ω evaluated at the minimum of $V_{\text{eff}}^{\text{trunc}}$), but $\hat{\Omega}_0$ is a $N_{\text{loops}} \times N_{\text{loops}}$ matrix! In practice, it cannot be calculated in loop space as a loop joining matrix; it would require generating all loops with length $2l_{\text{max}} - 2$ or less¹⁰. However, at the minimum, it can be obtained from the planar master field ϕ_α^0 as:

$$\hat{\Omega}_0(C, C') = \sum_{A=1}^2 \sum_{a,b=1}^N \left(\left. \frac{\partial \phi^\dagger(C)}{\partial (X_A^\dagger)_{ab}} \right) \right|_{\phi_\alpha^0} \left(\left. \frac{\partial \phi(C')}{\partial (X_A)_{ba}} \right) \right|_{\phi_\alpha^0}, \quad C, C' = 1, \dots, N_{\text{loops}}$$

A simple analysis of small fluctuations yields for the spectrum eigenvalues:

$$\epsilon_n = \left[\text{eig}_n \left(\sum_{C'=1}^{N_{\text{loops}}} \hat{\Omega}_0(C, C') V_0^{(2)}(C', C'') \right) \right]^{1/2} \quad (7)$$

As a result of the difference in dimensions between $\hat{\Omega}_0$ and Ω_0 , there are N_Ω physical, and in general finite, eigenvalues, with $N_{\text{loops}} - N_\Omega$ zero eigenvalues [44, 46]¹¹.

¹⁰For the truncated system with $l_{\text{max}} = 14$, one would have to identify loops containing up to 26 matrices.

¹¹It is straightforward to show that the finite eigenvalues of the $2N^2 \times 2N^2$ matrix $\mathcal{M}_{ab, a'b'} = \sum_{C, C'} \left(\left. \frac{\partial \phi(C')}{\partial (X_A)_{ba}} \right) \right|_{\phi_\alpha^0} V_0^{(2)}(C, C') \left(\left. \frac{\partial \phi^\dagger(C)}{\partial (X_A^\dagger)_{a'b'}} \right) \right|_{\phi_\alpha^0}$ map to (the square of the) finite eigenvalues of (7). We check at every run that the two sets of eigenvalues are identical. Motivation as to why this mass matrix can also be considered is given in [44, 46].

3 Massless quantum mechanical system

In this section we consider the two hermitian matrices (X_1 and X_2) system Hamiltonian

$$\hat{H} = \frac{1}{2} \sum_{A=1}^2 \text{Tr} P_A^2 - \frac{g_{YM}^2}{N} \text{Tr}[X_1, X_2]^2. \quad (8)$$

P_A is canonical conjugate to X_A , $A = 1, 2$. This system has one dimensional parameter only, g_{YM} ¹². Its dimension and that of the fields X_A are:

$$[g_{YM}] = \frac{3}{2}, \quad [X_1] = [X_2] = -\frac{1}{2}.$$

As such, we expect a simple algebraic dependence on g_{YM} of all physical quantities, simply determined by their dimensions. For instance,

$$e = \Lambda_e g_{YM}^{2/3}, \quad \text{Tr} X_1^2 = \Lambda_{[11]} g_{YM}^{-2/3}, \quad \text{Tr} X_1^4 = \Lambda_{[1111]} g_{YM}^{-4/3}, \quad \text{etc.},$$

where e is any energy of the system.

We considered 15 values of g_{YM} , ranging from 1 to 12, chosen so that they are reasonably distributed over this range in both a linear and logarithmic scale, as shown in Table 2:

g_{YM}														
1	1.28403	1.64872	2	2.6	3.25	4	5	6	7	8	9	10	11	12

Table 2: Values of g_{YM} . Note that $1.28403 \equiv \exp 0.25$, $1.64872 \equiv \exp 0.50$.

For each value of g_{YM} , and directly in this massless limit, we found that the optimization algorithm exhibited remarkable stable convergence to the system's minimum. When physical properties are plotted as functions of g_{YM} , they show remarkable agreement with their predicted scaling dependence. We present these results in the next subsections, first for large N planar quantities, and then for the spectrum of the theory.

3.1 Planar limit

Table 3 displays a subset of the results obtained for the planar limit of the quantum mechanical system: the ground state large N energy, the expectation values of all loops with 4 matrices or less, and an "angle", details of which will be given in the following. Following the discussion in Appendix A, we list the ground state energies with 5 decimal places. Loop data is shown with 4 decimal places, as to this accuracy loops odd under $1 \rightarrow -1$ and $2 \rightarrow -2$ vanish, and the symmetry $1 \leftrightarrow 2$ is realized¹³.

¹²Recall that in terms of our conventions, 't Hooft's coupling $\lambda = g_{YM}^2$.

¹³Only in very few cases is this not the case, and even in those cases the discrepancy is $\sim 1 \times 10^{-4}$.

3.1.1 $U(1)$ charges

As is known, the system (8) has a global $SO(2) \simeq U(1)$ symmetry associated with rotations of the two hermitian matrices X_1 and X_2 , with generator

$$\hat{L} = -i \text{Tr} \left(X_1 \frac{\partial}{\partial X_2} - X_2 \frac{\partial}{\partial X_1} \right).$$

In terms of complex matrices $Z \equiv X_1 + iX_2$, $Z^\dagger \equiv X_1 - iX_2$,

$$Z \rightarrow e^{i\phi} Z, \quad Z^\dagger \rightarrow e^{-i\phi} Z^\dagger, \quad \hat{L} = \text{Tr} \left(Z \frac{\partial}{\partial Z} - Z^\dagger \frac{\partial}{\partial Z^\dagger} \right).$$

At the planar level, expectation values of correlators with non-zero $U(1)$ charges should vanish. In order to evidence this, we display the expectation values of all loops with 4 complex matrices or less in table 4. The vanishing of all listed non-zero charge planar correlators is realized to within at least 5 significant figures¹⁴.

3.1.2 Scaling behaviour

In figure 1, a plot of large N ground state energies versus g_{YM} is shown. We fit

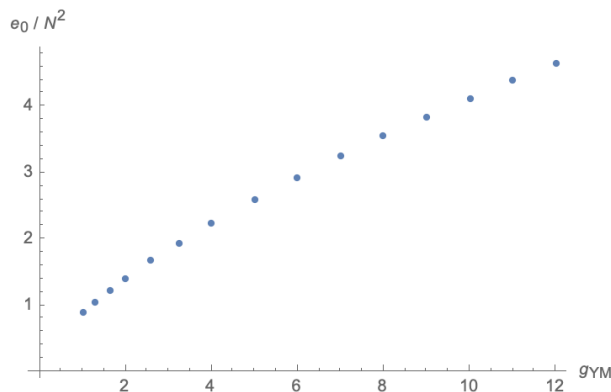


Figure 1: Planar ground state energies e_0/N^2 versus g_{YM}

the data to the curve

$$e_0/N^2 = A_0 g_{YM}^p,$$

by performing a linear regression (least squares) fit to the logarithmic plot. We find:

$$\ln A_0 = -0.117625(8), \quad p = 0.666671(5).$$

This linear fit is shown in Figure 2.

¹⁴We do not display the imaginary part of the generically complex loops, as these are numerically zero to at least 4 decimal places for the loops presented in table 4. The fact that their imaginary part is numerically zero follows from the vanishing of loops in table 3 that are odd under $1 \rightarrow -1$ or $2 \rightarrow -2$.

g_{YM}	1.0	1.28403	1.64872	2.0	2.6	3.25	4.0	5.0	6.0	7.0	8.0	9.0	10.0	11.0	12.0
e_0/N^2	0.88904	1.05027	1.24075	1.41124	1.68099	1.95060	2.24021	2.59951	2.93549	3.25320	3.55622	3.84669	4.12662	4.39716	4.65995
$\text{Tr } 1/N$	1.0000	1.0000	1.0000	1.0000	1.0000	1.0000	1.0000	1.0000	1.0000	1.0000	1.0000	1.0000	1.0000	1.0000	1.0000
$[1]/N^{3/2}$	0.0000	0.0000	0.0000	0.0000	0.0001	0.0000	0.0000	0.0000	0.0000	0.0000	-0.0001	0.0000	-0.0001	0.0000	0.0000
$[2]/N^{3/2}$	0.0000	0.0000	0.0003	0.0000	0.0000	0.0000	0.0000	0.0000	0.0000	0.0000	0.0000	0.0000	0.0000	0.0000	0.0000
$[11]/N^2$	0.4651	0.3937	0.3333	0.2931	0.2460	0.2120	0.1846	0.1591	0.1409	0.1271	0.1163	0.1075	0.1002	0.0941	0.0887
$[12]/N^2$	0.0000	0.0000	0.0000	0.0000	0.0000	0.0000	0.0000	0.0000	0.0000	0.0000	0.0000	0.0000	0.0000	0.0000	0.0000
$[22]/N^2$	0.4651	0.3937	0.3333	0.2930	0.2460	0.2120	0.1846	0.1591	0.1409	0.1271	0.1163	0.1075	0.1002	0.0941	0.0887
$[111]/N^{5/2}$	0.0000	0.0000	0.0001	0.0000	0.0001	0.0000	0.0000	0.0000	0.0000	0.0000	-0.0001	0.0000	0.0000	0.0000	0.0000
$[112]/N^{5/2}$	0.0000	0.0000	0.0001	0.0000	0.0000	0.0000	0.0000	0.0000	0.0000	0.0000	0.0000	0.0000	0.0000	0.0000	0.0000
$[122]/N^{5/2}$	0.0000	0.0000	0.0000	0.0000	0.0000	0.0000	0.0000	0.0000	0.0000	0.0000	0.0000	0.0000	0.0000	0.0000	0.0000
$[222]/N^{5/2}$	-0.0001	0.0000	0.0003	0.0000	0.0000	0.0000	0.0000	0.0000	0.0000	0.0000	0.0000	0.0000	0.0000	0.0000	0.0000
$[1111]/N^3$	0.4364	0.3127	0.2241	0.1732	0.1221	0.0907	0.0687	0.0511	0.0400	0.0326	0.0273	0.0233	0.0203	0.0178	0.0159
$[1112]/N^3$	0.0000	0.0000	0.0000	0.0000	0.0000	0.0000	0.0000	0.0000	0.0000	0.0000	0.0000	0.0000	0.0000	0.0000	0.0000
$[1122]/N^3$	0.1949	0.1396	0.1001	0.0773	0.0545	0.0405	0.0307	0.0228	0.0179	0.0146	0.0122	0.0104	0.0090	0.0080	0.0071
$[1212]/N^3$	0.0467	0.0334	0.0240	0.0185	0.0131	0.0097	0.0074	0.0055	0.0043	0.0035	0.0029	0.0025	0.0022	0.0019	0.0017
$[1222]/N^3$	0.0000	0.0000	0.0000	0.0000	0.0000	0.0000	0.0000	0.0000	0.0000	0.0000	0.0000	0.0000	0.0000	0.0000	0.0000
$[2222]/N^3$	0.4364	0.3127	0.2241	0.1732	0.1221	0.0907	0.0687	0.0511	0.0400	0.0326	0.0273	0.0233	0.0202	0.0178	0.0159
"angle"	0.68489	0.68488	0.68482	0.68478	0.68477	0.68472	0.68474	0.68472	0.68472	0.68471	0.68518	0.68513	0.68516	0.68466	0.68516

Table 3: Planar numerical results obtained with a truncation to 2615 loops ($l_{\max} = 14$) with Ω a 93×93 matrix.

l	$g_{\gamma M}$	1,00	1,28	1,65	2,00	2,60	3,25	4,00	5,00	6,00	7,00	8,00	9,00	10,00	11,00	12,00
0	Energy	0.88904	1.05027	1.24075	1.41124	1.68099	1.95060	2.24021	2.59951	2.93549	3.25320	3.55622	3.84669	4.12662	4.39716	4.65995
0	$\text{Tr}1/N$	1.0000	1.0000	1.0000	1.0000	1.0000	1.0000	1.0000	1.0000	1.0000	1.0000	1.0000	1.0000	1.0000	1.0000	1.0000
1	$[Z]/N^{3/2}$	0.0000	0.0000	0.0000	0.0000	0.0000	-0.0000	0.0000	0.0000	0.0000	-0.0001	-0.0000	-0.0000	-0.0000	-0.0000	0.0000
-1	$[Z^\dagger]/N^{3/2}$	0.0000	0.0000	0.0000	0.0000	0.0000	-0.0000	0.0000	0.0000	0.0000	-0.0001	-0.0000	-0.0000	-0.0000	-0.0000	0.0000
2	$[ZZ]/N^2$	0.0000	0.0000	-0.0000	0.0000	-0.0000	-0.0000	0.0000	-0.0000	-0.0000	0.0000	-0.0000	0.0000	0.0000	-0.0000	0.0000
0	$[ZZ^\dagger]/N^2$	0.9303	0.7874	0.6665	0.5861	0.4920	0.4240	0.3692	0.3182	0.2818	0.2542	0.2325	0.21500	0.2004	0.1881	0.1774
-2	$[Z^\dagger Z^\dagger]/N^2$	0.0000	0.0000	-0.0000	0.0000	-0.0000	-0.0000	0.0000	-0.0000	-0.0000	0.0000	0.0000	0.0000	-0.0000	0.0000	0.0000
3	$[Z^3]/N^{5/2}$	0.0000	0.0000	0.0000	0.0000	-0.0000	0.0000	-0.0000	-0.0000	0.0000	-0.0000	-0.0000	-0.0000	0.0000	0.0000	-0.0000
1	$[ZZZ^\dagger]/N^{5/2}$	0.0000	0.0000	0.0000	0.0000	0.0000	-0.0000	0.0000	0.0000	0.0000	0.0000	-0.0000	-0.0000	-0.0000	-0.0000	-0.0000
-1	$[ZZ^\dagger Z^\dagger]/N^{5/2}$	0.0000	0.0000	0.0000	0.0000	0.0000	-0.0000	0.0000	0.0000	0.0000	0.0000	-0.0000	-0.0000	-0.0000	-0.0000	-0.0000
-3	$[Z^\dagger Z^\dagger Z^\dagger]/N^{5/2}$	0.0000	0.0000	0.0000	0.0000	-0.0000	0.0000	-0.0000	-0.0000	-0.0000	-0.0000	-0.0000	-0.0000	0.0000	0.0000	-0.0000
4	$[ZZZZ]/N^3$	0.0000	0.0000	0.0000	-0.0000	0.0000	-0.0000	0.0000	-0.0000	-0.0000	-0.0000	-0.0000	0.0000	0.0000	0.0000	-0.0000
2	$[ZZZZ^\dagger]/N^3$	0.0000	0.0000	-0.0000	0.0000	0.0000	0.0000	0.0000	0.0000	-0.0000	-0.0000	-0.0000	-0.0000	0.0000	0.0000	0.0000
0	$[ZZZ^\dagger Z^\dagger]/N^3$	0.9662	0.6923	0.4961	0.3835	0.2703	0.2008	0.1522	0.1130	0.0886	0.0722	0.0604	0.0515	0.0448	0.0395	0.0352
0	$[Z^\dagger Z^\dagger Z^\dagger]/N^3$	1.5589	1.11698	0.8004	0.6187	0.4361	0.3239	0.2456	0.1824	0.1430	0.1164	0.0974	0.0832	0.0723	0.0637	0.0567
-2	$[Z^\dagger Z^\dagger Z^\dagger]/N^3$	0.0000	0.0000	-0.0000	0.0000	0.0000	0.0000	0.0000	0.0000	-0.0000	-0.0000	-0.0000	-0.0000	0.0000	0.0000	0.0000
-4	$[Z^\dagger Z^\dagger Z^\dagger Z^\dagger]/N^3$	0.0000	0.0000	-0.0000	0.0000	0.0000	0.0000	0.0000	0.0000	-0.0000	-0.0000	-0.0000	-0.0000	0.0000	0.0000	0.0000

Table 4: Real part of planar expectation values of correlators built with complex matrices and $U(1)$ charges l .

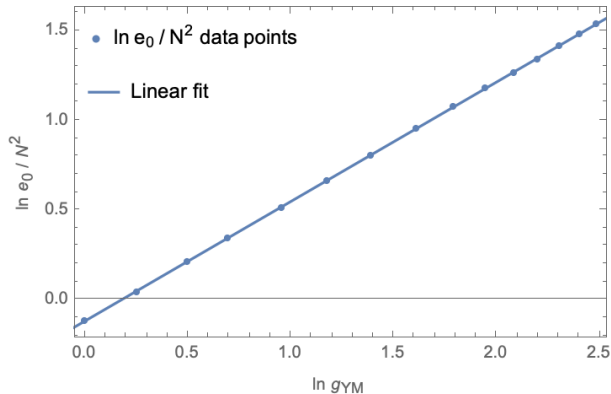


Figure 2: Linear fit to $\ln e_0/N^2$ versus $\ln g_{YM}$

The accuracy with which the interpolation matches the exact scaling $p = 2/3$ at this level of truncation is remarkable¹⁵. We are then justified in setting $p = 2/3$ and fit the data to the scaling function

$$e_0/N^2 = \Lambda_0 g_{YM}^{2/3}, \quad \left(= \Lambda_0 \lambda^{1/3} \right) \quad (9)$$

with result

$$\Lambda_0 = 0.889034(3). \quad (10)$$

Figure 3 displays the fit of the large N planar ground state energies to the scaling function (9) with parameter (10). Again, the level of accuracy (10) with which the numerically obtained planar ground state energies match the scaling behaviour (9) at this level of truncation is remarkable.

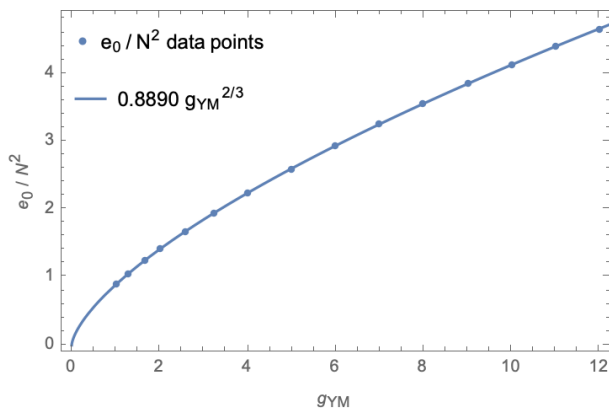


Figure 3: Numerically obtained large N ground state energies and fit to the scaling function $e_0/N^2 = 0.8890 g_{YM}^{2/3}$

Taking into account possible truncation dependent errors, as estimated in

¹⁵The parameters and their uncertainties are obtained with the Mathematica functions LinearModelFit and NonlinearModelFit. Note that the fit uncertainties are remarkably consistent with the estimated numerical errors associated with this level of loop truncation.

Appendix A, we then list the final scaling dependence on 't Hooft's coupling for the planar ground state energy of the massless system as:

$$e_0/N^2 = 0.8890(2) \lambda^{1/3}$$

We follow the same analysis for loops with two matrices and consider the correlator $\text{Tr}(Z^\dagger Z)/N^2 = (\text{Tr}X_1^2 + \text{Tr}X_2^2)/N^2$. The logarithmic g_{YM} dependence is first approximated by a linear fit, and then matched to the scaling dimensions of the loop correlator:

$$\text{Tr}(Z^\dagger Z)/N^2 = A_{Z^\dagger Z} g_{YM}^p, \quad \text{and then } \text{Tr}(Z^\dagger Z)/N^2 = \Lambda_{Z^\dagger Z} g_{YM}^{-2/3}.$$

The results are presented in table 5 and displayed in Figure 4.

Parameters of (log) linear fit		$p = -2/3$ fixed	Final scaling function
$\ln A_{Z^\dagger Z}$	p	$\Lambda_{Z^\dagger Z}$	$\text{Tr}(Z^\dagger Z)/N^2$
-0.07219(7)	-0.66672(4)	0.93027(3)	$0.930(1) \lambda^{-1/3}$

Table 5: $\text{Tr}(Z^\dagger Z)/N^2$ log linear fit parameters and scaling parameter $\Lambda_{Z^\dagger Z}$ at this level of truncation. The scaling parameter in the final scaling function takes into account estimated effects of the loop truncation.

The scaling power for the large N planar correlator is again predicted with a high level of accuracy, and their numerical values match with a high level of precision the scaling behaviour. The numerical errors associated with the loop truncation are estimated in Appendix A, and taken into account in the final scaling function presented in table 5.

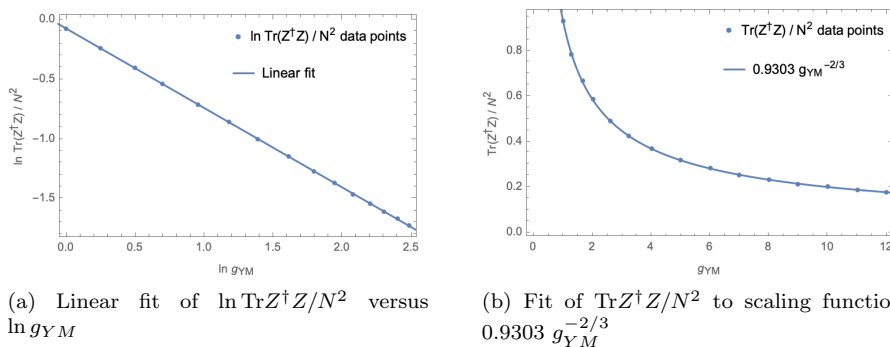


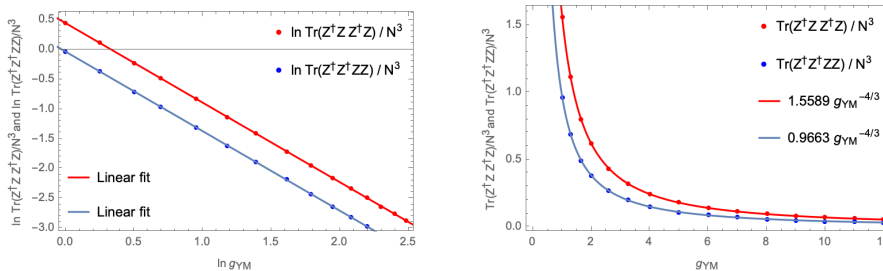
Figure 4: Numerical results for the planar limit of $\text{Tr}Z^\dagger Z/N^2$, logarithmic linear fit and fit to predicted scaling dependence.

For invariant loops with 4 matrices, we consider the loops $\text{Tr}(Z^\dagger Z Z^\dagger Z)/N^3$ and $\text{Tr}(Z^\dagger Z^\dagger Z Z)/N^3$, and carry out the same analysis, which is summarized in table 6 and figure 5.

Remarks similar to those given for the previously discussed large N planar quantities which concern the high level of accuracy of the numerical results, apply to the invariant loops with 4 matrices considered in this case too.

	Log linear fit		$p = -4/3$	Final
	$\ln A$	p	Λ	Scaling function
$\text{Tr}(Z^\dagger Z Z^\dagger Z)/N^3$	0.4441(1)	-1.33340(6)	1.55895(8)	$1.559(8) \lambda^{-2/3}$
$\text{Tr}(Z^\dagger Z^\dagger Z Z)/N^3$	-0.0342(2)	-1.3334(1)	0.96626(8)	$0.966(4) \lambda^{-2/3}$

Table 6: Logarithmic linear fit parameters and scaling parameter for $\text{Tr}(Z^\dagger Z Z^\dagger Z)/N^3$ and $\text{Tr}(Z^\dagger Z^\dagger Z Z)/N^3$.



(a) Linear fit of the log of 4 matrices loop expectation values versus $\ln g_{YM}$

(b) Fit of loops of 4 matrices to scaling functions $\Lambda g_{YM}^{-4/3}$

Figure 5: Numerical results for the planar limit of $\text{Tr}(Z^\dagger Z Z^\dagger Z)/N^3$ and $\text{Tr}(Z^\dagger Z^\dagger Z Z)/N^3$, logarithmic linear fits and fits to predicted scaling dependence.

Finally, we consider an "angle" defined to be

$$\mathcal{A} \equiv N \frac{\text{Tr} X_1^2 X_2^2 - \text{Tr} X_1 X_2 X_1 X_2}{\text{Tr} X_1^2 \text{Tr} X_2^2} = -\frac{N \text{Tr}[X_1, X_2]^2}{2 \text{Tr} X_1^2 \text{Tr} X_2^2}.$$

For the integral with masses, and at large coupling, it has been shown that the two matrices commute [47]. For the quantum mechanical system in the massless limit, we observe, from the data listed in 3 that this ratio remains constant, and we obtain

$$\mathcal{A} = 0.68487(5).$$

Again, taking into account possible numerical errors associated with the loop truncation, we obtain

$$\mathcal{A} = N \frac{\text{Tr} X_1^2 X_2^2 - \text{Tr} X_1 X_2 X_1 X_2}{\text{Tr} X_1^2 \text{Tr} X_2^2} = 0.685(2).$$

In [42], the large N YM quantum mechanics of two matrices with mass was considered, and it was there pointed out that this ratio seemed to show convergence to a constant value at large coupling. We have been able to establish what its value is directly in the massless limit, for all coupling values, with a high degree of accuracy.

3.2 $1/N$ spectrum

We consider in this subsection the numerical results obtained for the spectrum of the theory. These are independent of N and are determined from the quadratic hamiltonian $H_{\text{trunc}}^{(2)}$ as $1/N$ fluctuations about the large N planar background, as described in Section 2.3.

3.2.1 Masses and scaling behaviour

We observe that the mass of the third excited state and of all other higher excited states show the expected increase with coupling. The same is not the case for the two lowest lying states. We will first concentrate on the third and higher excited states, and discuss the two lowest lying states at the end of this subsection.

Numerically, one finds that the lowest lying states are determined quite accurately for small loop truncations, with the next higher lying states then becoming more accurate with larger number loops, and so on.

Table 7 displays the numerical results obtained for the masses of the 3rd to the 37th excited state¹⁶ as a function of the coupling constant g_{YM} . Numerically, one finds that the lowest lying states are determined quite accurately for small loop truncations, with the next higher lying states then becoming more accurate with a larger number loops, and so on. Although the code generates data for all first 93 excited states, we have chosen to list masses up to the 37th excited state as their masses are stable at this level of truncation. Truncation error estimates are presented in Appendix A.

We then carry out a similar analysis to that of previous subsection, by first performing a linear fit to the dependence of $\ln e_n, n = 3, \dots, 37$ on the logarithm of g_{YM} , comparing it with the the scaling power prediction, and then optimize the match to the scaling dependence of the energies:

$$e_n = A_n g_{YM}^p, \quad \text{and then } e_n = \Lambda_n g_{YM}^{2/3}.$$

The Λ_n are then adjusted to take into account truncation error estimates. The results are presented in table 8¹⁷.

Again we observe an excellent agreement with the expected scaling power $2/3$ of the coupling constant g_{YM} for the masses of the excited states, typically with uncertainties below the 1% level¹⁸. The two degenerate massive lowest lying states e_3 and e_4 , of particular physical relevance, are specially accurate.

In figures 6 , 7 and 8, we display the logarithmic linear fits and the fits to the scaling power law of the numerical spectrum data for $e_n, n = 3, \dots, 15$. This illustrates the patterns of degeneracy, which will be further discussed in the next subsection.

¹⁶These would be 2 particle states to 6 particle states in the free system with a mass coupling.

¹⁷The somewhat unconventional notation 4.62(21) say, instead of 4.6(2), is meant to help compare final parameter error estimates with those of the current (2615 loops) truncation level (in this case 4.62(2)) and highlight possible differences within possible multiplets.

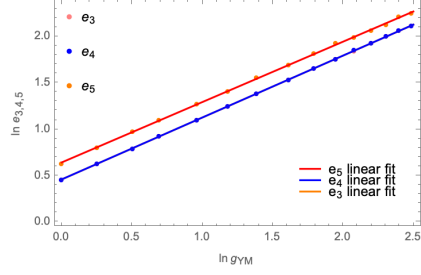
¹⁸The mass e_{12} is an intriguing discrepancy that may require further later re-examination. However, the quality of its fit to the scaling power law is in line with other excited states.

g_{YM}	1.0	1.28403	1.64872	2.0	2.6	3.25	4.0	5.0	6.0	7.0	8.0	9.0	10.0	11.0	12.0
e_3	1.58783	1.87590	2.21627	2.52042	3.00208	3.48335	4.00097	4.64009	5.24314	5.80891	6.35076	6.87178	7.36991	7.84974	8.32061
e_4	1.58826	1.87666	2.21658	2.52084	3.00301	3.48399	4.00108	4.64333	5.24456	5.80914	6.35230	6.87266	7.37212	7.85155	8.32270
e_5	1.8817	2.2384	2.6469	2.9897	3.5754	4.1113	4.7403	5.4561	6.1860	6.8548	7.2816	7.8399	8.4051	9.1596	9.5306
e_6	2.3624	2.8549	3.3788	3.6678	4.5283	5.2501	6.0686	6.9439	7.8667	8.6501	9.4171	10.217	10.864	11.630	12.340
e_7	2.4227	2.8614	3.3845	3.8005	4.5699	5.2754	6.0982	7.0592	8.0208	8.7401	9.5187	10.368	11.175	11.731	12.574
e_8	2.8920	3.5499	4.2006	4.5165	5.6054	6.4257	7.4950	8.5833	9.7959	10.620	11.343	12.400	13.159	14.118	14.850
e_9	3.0224	3.5679	4.2135	4.7529	5.6196	6.5906	7.6095	8.7697	9.9158	10.999	11.722	12.656	13.328	14.740	15.106
e_{10}	3.1770	3.7796	4.4787	4.9936	6.0322	6.9061	8.0139	9.2056	10.538	11.536	12.659	13.720	14.655	15.607	16.529
e_{11}	3.2119	3.7908	4.4854	5.0488	6.0746	7.0056	8.0833	9.2782	10.605	11.620	12.732	13.763	14.762	15.718	16.576
e_{12}	3.6644	4.3828	5.2722	5.7622	7.0210	8.1770	9.3819	10.537	12.173	13.366	13.179	14.243	15.329	17.050	17.522
e_{13}	3.7820	4.5010	5.3748	5.9431	7.2252	8.2713	9.4737	10.789	12.494	13.589	15.134	16.433	17.470	18.407	19.565
e_{14}	3.9256	4.5641	5.4285	6.0557	7.3141	8.4786	9.8013	11.268	12.813	13.813	15.230	16.737	17.774	18.540	19.990
e_{15}	3.9768	4.6918	5.5272	6.1198	7.5254	8.6510	10.060	11.526	13.202	14.089	15.555	16.916	18.021	18.930	20.128
e_{16}	3.9904	4.7478	5.6144	6.3157	7.5563	8.7746	10.124	11.600	13.250	14.597	15.666	16.972	18.166	19.639	20.415
e_{17}	4.2782	5.1428	6.0890	6.7240	8.1507	9.1677	10.767	12.325	13.917	15.308	17.491	18.728	20.168	20.714	22.509
e_{18}	4.7181	5.5377	6.6292	7.1827	8.8371	10.081	11.790	13.342	15.513	16.652	18.382	19.823	21.356	22.874	23.684
e_{19}	4.7579	5.6074	6.6581	7.4679	8.9802	10.353	11.879	13.656	15.716	17.144	18.613	20.155	21.445	23.092	24.225
e_{20}	4.7994	5.6289	6.6876	7.5628	9.1130	10.473	12.018	13.895	15.768	17.276	18.952	20.882	22.208	23.219	25.016
e_{21}	4.8160	5.6543	6.7112	7.6996	9.1279	10.549	12.048	13.920	15.935	17.511	19.144	20.921	22.451	23.420	25.119
e_{22}	5.0709	5.8664	7.0180	7.9112	9.4813	11.056	12.703	14.521	16.572	18.178	19.980	21.713	23.141	24.453	26.087
e_{23}	5.1189	5.9758	7.1513	8.0451	9.6420	11.162	12.899	14.915	16.728	18.454	20.172	21.979	23.337	24.548	26.198
e_{24}	5.5177	6.4132	7.7126	8.6924	10.400	11.973	13.669	15.655	18.175	19.692	21.818	23.843	25.621	26.910	28.568
e_{25}	5.5663	6.5097	7.7646	8.8801	10.577	12.156	14.062	15.994	18.407	20.141	22.037	24.103	25.747	27.387	29.097
e_{26}	5.6155	6.6611	7.8974	8.9917	10.701	12.409	14.195	16.348	18.606	20.372	22.472	24.597	26.309	27.733	29.533
e_{27}	5.6549	6.7057	7.9368	8.9654	10.722	12.487	14.344	16.464	18.706	20.675	22.619	24.643	26.417	27.766	29.735
e_{28}	5.9041	6.8887	8.2739	9.4674	11.256	12.937	14.844	16.996	19.266	21.269	23.800	25.686	27.749	29.054	31.282
e_{29}	6.0821	7.0254	8.3083	9.4841	11.329	13.063	15.009	17.416	19.623	21.800	24.063	26.090	27.884	29.207	31.400
e_{30}	6.1661	7.1322	8.5372	9.6920	11.623	13.387	15.364	17.831	20.078	22.169	24.848	26.217	28.152	29.996	31.865
e_{31}	6.3174	7.5318	8.8912	9.9197	11.876	13.525	15.821	18.185	20.581	22.576	25.696	28.703	30.412	30.253	34.036
e_{32}	6.4214	7.7110	9.0560	10.269	12.467	14.282	16.409	18.871	21.506	23.665	26.221	28.788	30.709	32.035	34.632
e_{33}	6.4975	7.7573	9.0860	10.373	12.514	14.618	16.617	19.174	21.600	23.724	26.621	29.246	31.143	32.371	35.148
e_{34}	6.7837	8.0036	9.4812	10.756	12.904	14.845	16.954	19.663	22.339	24.689	26.737	29.415	31.332	33.115	35.432
e_{35}	6.7997	8.0186	9.4927	10.793	12.944	14.877	17.047	19.847	22.377	24.816	27.003	29.730	31.483	33.359	35.767
e_{36}	6.9259	8.0801	9.6280	10.935	13.037	15.090	17.302	19.985	22.726	24.963	27.355	29.820	32.145	33.537	36.135
e_{37}	7.0077	8.2133	9.7493	11.030	13.209	15.377	17.472	20.177	23.011	25.253	27.864	29.948	32.250	34.672	36.447

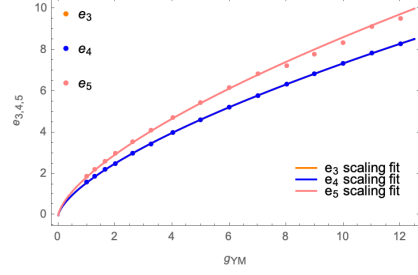
Table 7: Numerical results for the spectrum with a truncation to 2615 loops ($l_{\max} = 14$) with Ω a 93×93 matrix. Only the states $n = 3, \dots, 37$ are listed.

	Log linear fit		$p = 2/3$ fixed	Final
n	$\ln A_n$	p	Λ_n	Scaling function
e_3	0.4624(1)	0.66657(7)	1.58767(9)	1.588(1) $\lambda^{1/3}$
e_4	0.4627(1)	0.66656(6)	1.58806(8)	1.588(1) $\lambda^{1/3}$
e_5	0.645(6)	0.650(3)	1.862(8)	1.86(3) $\lambda^{1/3}$
e_6	0.873(6)	0.660(4)	2.373(8)	2.37(3) $\lambda^{1/3}$
e_7	0.885(3)	0.661(2)	2.406(5)	2.41(3) $\lambda^{1/3}$
e_8	1.09(1)	0.651(6)	2.91(2)	2.91(11) $\lambda^{1/3}$
e_9	1.112(7)	0.652(4)	2.98(1)	2.98(10) $\lambda^{1/3}$
e_{10}	1.159(3)	0.663(2)	3.170(5)	3.17(2) $\lambda^{1/3}$
e_{11}	1.167(2)	0.662(1)	3.191(5)	3.19(2) $\lambda^{1/3}$
e_{12}	1.34(2)	0.62(1)	3.57(5)	3.57(18) $\lambda^{1/3}$
e_{13}	1.336(6)	0.660(3)	3.77(1)	3.77(6) $\lambda^{1/3}$
e_{14}	1.361(5)	0.657(3)	3.85(1)	3.85(7) $\lambda^{1/3}$
e_{15}	1.382(7)	0.655(4)	3.92(2)	3.92(8) $\lambda^{1/3}$
e_{16}	1.393(4)	0.657(3)	3.97(1)	3.97(6) $\lambda^{1/3}$
e_{17}	1.457(9)	0.663(5)	4.27(2)	4.27(4) $\lambda^{1/3}$
e_{18}	1.547(7)	0.656(4)	4.62(2)	4.62(15) $\lambda^{1/3}$
e_{19}	1.563(3)	0.656(2)	4.70(1)	4.70(10) $\lambda^{1/3}$
e_{20}	1.567(4)	0.663(2)	4.770(9)	4.77(7) $\lambda^{1/3}$
e_{21}	1.572(3)	0.665(2)	4.802(8)	4.80(7) $\lambda^{1/3}$
e_{22}	1.615(4)	0.663(2)	5.001(9)	5.00(12) $\lambda^{1/3}$
e_{23}	1.633(4)	0.659(2)	5.07(1)	5.07(13) $\lambda^{1/3}$
e_{24}	1.701(5)	0.664(3)	5.46(1)	5.46(10) $\lambda^{1/3}$
e_{25}	1.716(3)	0.665(2)	5.547(9)	5.55(11) $\lambda^{1/3}$
e_{26}	1.728(3)	0.666(2)	5.631(8)	5.63(6) $\lambda^{1/3}$
e_{27}	1.735(2)	0.666(1)	5.666(6)	5.67(7) $\lambda^{1/3}$
e_{28}	1.776(6)	0.666(3)	5.90(1)	5.90(16) $\lambda^{1/3}$
e_{29}	1.790(4)	0.665(2)	5.98(1)	5.98(16) $\lambda^{1/3}$
e_{30}	1.812(4)	0.664(3)	6.10(1)	6.10(20) $\lambda^{1/3}$
e_{31}	1.83(1)	0.673(8)	6.32(4)	6.32(33) $\lambda^{1/3}$
e_{32}	1.866(5)	0.673(3)	6.52(2)	6.52(33) $\lambda^{1/3}$
e_{33}	1.874(6)	0.675(4)	6.59(2)	6.59(29) $\lambda^{1/3}$
e_{34}	1.916(3)	0.663(2)	6.76(1)	6.76(30) $\lambda^{1/3}$
e_{35}	1.917(3)	0.666(2)	6.793(9)	6.79(22) $\lambda^{1/3}$
e_{36}	1.930(3)	0.664(2)	6.87(1)	6.87(26) $\lambda^{1/3}$
e_{37}	1.943(3)	0.665(2)	6.960(9)	6.96(26) $\lambda^{1/3}$

Table 8: Log linear fit parameters and scaling parameters Λ_n for $n = 3, \dots, 37$ at this level of truncation. The scaling parameter in the final scaling function takes into account estimated effects of the loop truncation.

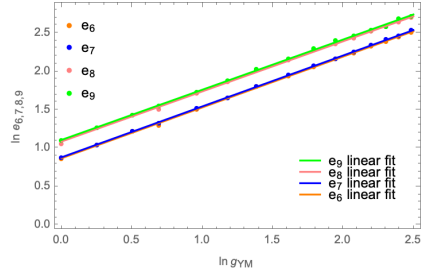


(a) Linear fit of the log of the $n = 3, 4, 5$ masses versus $\ln g_{YM}$

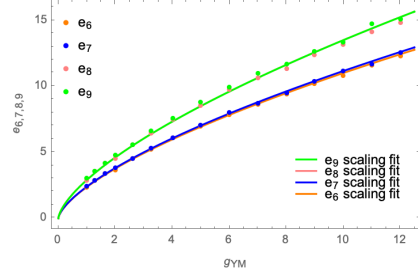


(b) Fit of the $n = 3, 4, 5$ masses to scaling functions $\Lambda_{3,4,5}^{2/3} g_{YM}$

Figure 6: Numerical results for the masses $e_{3,4,5}$: logarithmic linear fits and fits to predicted scaling dependence. Note that e_3 is not visible due to the degeneracy with e_4

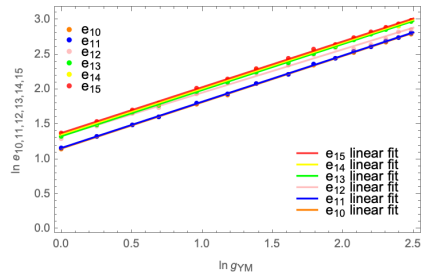


(a) Linear fit of the log of the $n = 6, 7, 8, 9$ masses versus $\ln g_{YM}$

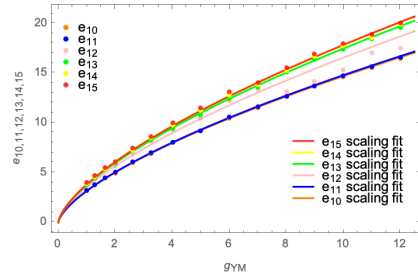


(b) Fit of $n = 6, 7, 8, 9$ masses to scaling function $\Lambda_{6,7,8,9}^{2/3} g_{YM}$

Figure 7: Numerical results for the masses $e_{6,7,8,9}$: logarithmic linear fits and fits to predicted scaling dependence. Two 2-fold degenerate states are apparent.



(a) Linear fit of the log of the $n = 10, \dots, 15$ masses versus $\ln g_{YM}$



(b) Fit of the $n = 10, \dots, 15$ masses to scaling function $\Lambda_{10,11,12,13,14,15}^{2/3} g_{YM}$

Figure 8: Numerical results for the masses $e_{10,11,12,13,14,15}$: logarithmic linear fits and fits to predicted scaling dependence.

3.2.2 $U(1)$ charges

The assignment of $U(1)$ charges to the different multiplets is more cleanly carried out in a complex matrices loop basis:

$$\begin{aligned}
[ZZ] &= [11] + 2i[12] - [22] \\
[ZZ^\dagger] &= [11] + [22] \\
[Z^\dagger Z^\dagger] &= [11] - 2i[12] - [22] \\
[Z^3] &= [111] + 3i[112] - 3[122] - i[222] \\
[ZZZ^\dagger] &= [111] + i[112] + [122] + i[222] \\
[ZZ^\dagger Z^\dagger] &= [111] - i[112] + [122] - i[222] \\
[Z^\dagger Z^\dagger Z^\dagger] &= [111] - 3i[112] - 3[122] + i[222] \\
&\vdots
\end{aligned} \tag{11}$$

This defines a (complex valued) linear transformation between the complex matrices loop components of a mass eigenvector and its hermitian matrices loop components. It is block diagonal, and as such one can carry out the analysis for each sector of fixed particle number.

We find that the pattern of degeneracies is best evidenced by considering spectra corresponding to truncation subsectors within the $l_{\max} = 14$ planar background ([44]). In this subsection, we base our discussion on a $l_{\max} = 10$ truncation for $g_{YM} = 10$.

On general grounds, states with non-zero charges should come in doublets $\pm l$. It should be remembered, though, that the present numerical approach is based on hermitian matrices parametrized by real master variables. So typically, the eigenvector components are real. To obtain states of definite charge, the two degenerate eigenvectors have to first be expressed in a complex matrices loop component basis using (11) and then the linear combinations identified that yield two states of definite opposite charges.

To illustrate the procedure, we display in table 9 the $[11], [12], [22]$ components of the eigenvectors v^3, v^4 and v^5 . The states e_3 and e_4 are degenerate. As it can be observed from (11), they essentially "group" the real and imaginary parts of the $l = \pm 2$ states: $v_{[11]}^3 = -v_{[22]}^3, v_{[11]}^4 = -v_{[22]}^4$ with $v_{[12]}^{3,4}$ the imaginary part. For the singlet, one has $v_{[11]}^5 = v_{[22]}^5$ with no imaginary part.

	Doublet		Singlet
	v^3	v^4	v^5
[11]	0.0643	-0.0401	0.0055
[12]	0.0830	0.1247	0.0000
[22]	-0.0643	0.0403	0.0055

Table 9: The $[11], [12], [22]$ components of the eigenvectors corresponding to the states e_3, e_4, e_5

After re-writing the doublet states in a complex matrices loop component basis, one performs the linear combination required to obtain the (chiral) states of definite charge.

The choice of the linear combination coefficients is determined within the 2-particle sector, but they act on the full eigenvector. The first 13 components of the states are displayed in table 10. By construction, $\bar{v}_{[ZZ]}^3$ and $\bar{v}_{[Z^\dagger Z^\dagger]}^4$ are set to 1. The table confirms the vanishing of all other components (numerically less than 1%), except for $\bar{v}_{[ZZZZ^\dagger]}^3$ and $\bar{v}_{[ZZ^\dagger Z^\dagger Z^\dagger]}^4$. These 4-particle components also carry charges $l = \pm 2$, respectively, and their enhancement to about 9% results from the fact that the Hamiltonian, unlike the dilatation operator or upon radial quantization, is not number conserving.

	\bar{v}^3	\bar{v}^4
[ZZ]	1.000 +i0.000	0.000 +i0.000
[ZZ [†]]	-0.001 +i0.001	-0.001- i0.001
[Z [†] Z [†]]	0.000 +i0.000	1.000 +i0.000
[ZZZ]	0.000 +i0.000	0.001 +i0.002
[ZZZ [†]]	0.000 +i0.000	-0.005 -i0.006
[ZZ [†] Z [†]]	-0.005 +i0.006	0.000 -i0.000
[Z [†] Z [†] Z [†]]	0.001 -i0.002	0.000 -i0.000
[ZZZZ]	0.001 -i0.000	0.003 +i0.002
[ZZZZ [†]]	0.091 +i0.002	0.005 -i0.008
[ZZZ [†] Z [†]]	0.007 +i0.002	0.007 -i0.002
[ZZ [†] ZZ [†]]	0.002 +i0.002	0.002 -i0.002
[ZZ [†] Z [†] Z [†]]	0.005 +i0.008	0.091 -i0.002
[Z [†] Z [†] Z [†] Z [†]]	0.003 -i0.002	0.001 +i0.000
Charge	$l = 2$	$l = -2$

Table 10: Assignment of charges ± 2 to the 3-4 doublet. By construction, $\bar{v}_{[ZZ]}^3$ and $\bar{v}_{[Z^\dagger Z^\dagger]}^4$ are set to 1.

We consider now the next 4 states e_{6-9} . They appear as two doubly degenerate states. Their [111], [112], [122], [222] components are displayed in table 11. Again, they "encode" real and imaginary parts of definite charge states, as can be seen by inspection of (11) : $v_{[122]}^6 \simeq -3v_{[111]}^6$, $v_{[112]}^6 \simeq -3v_{[222]}^6$ and similarly for v^7 , whereas $v_{[122]}^8 \simeq v_{[111]}^8$, $v_{[112]}^8 \simeq v_{[222]}^8$, and similarly for v^9 .

	Doublet		Doublet	
	v^6	v^7	v^8	v^9
[111]	0.1403	-0.1403	-0.0238	0.0174
[112]	0.4269	0.4104	-0.0184	-0.0239
[122]	-0.4112	0.4225	-0.0243	0.0158
[222]	-0.1398	-0.1340	-0.0159	-0.0228

Table 11: The [111], [112], [122], [222] components of the eigenvectors corresponding to the states e_6, e_7, e_8, e_9

Expressing the doublet states in complex matrices loop components, and performing linear combinations within each doublet to obtain states of definite charge, one obtains table 12. Other than $\bar{v}_{[ZZZZ]}^6$, $\bar{v}_{[Z^\dagger Z^\dagger Z^\dagger]}^7$, $\bar{v}_{[ZZZZ^\dagger]}^8$, $\bar{v}_{[Z^\dagger Z^\dagger]}^9$, all

set to one, the other components vanish to within 3% for the $l = \pm 3$ doublet and within 5% for the $l = \pm 1$ doublet.

	Doublet		Doublet	
	\bar{v}^6	\bar{v}^7	\bar{v}^8	\bar{v}^9
$[ZZ]$	0.003+i0.000	-0.005 +i0.003	0.002 -i0.005	-0.006 -i0.015
$[ZZ^\dagger]$	-0.013 +i0.007	-0.013 -i0.007	0.007 +i0.011	0.007 -i0.011
$[Z^\dagger Z^\dagger]$	-0.005 -i0.003	0.003 -i0.000	-0.006 +i0.015	0.002 +i0.005
$[ZZZ]$	1.000 +i0.000	0.000 +i0.000	0.012 -i0.013	-0.008 +i0.001
$[ZZZ^\dagger]$	0.011 +i0.006	-0.003 -i0.005	1.000 +i0.000	0.000 +i0.000
$[ZZ^\dagger Z^\dagger]$	-0.003 +i0.005	0.011 -i0.006	0.000 +i0.000	1.000 +i0.000
$[Z^\dagger Z^\dagger Z^\dagger]$	0.000 +i0.000	1.000 +i0.000	-0.008 -i0.001	0.012 +i0.013
$[ZZZZ]$	0.004 -i0.008	-0.003 -i0.001	-0.017 +i0.060	0.003 +i0.033
$[ZZZZ^\dagger]$	-0.011 +i0.005	0.026 -i0.026	-0.003 +i0.015	-0.043 +i0.052
$[ZZZ^\dagger Z^\dagger]$	0.026 -i0.060	0.026 +i0.060	-0.005 -i0.026	-0.005 +i0.026
$[ZZ^\dagger Z^\dagger Z^\dagger]$	0.015 -i0.009	0.015 +i0.009	0.006 -i0.010	0.006 +i0.010
$[Z^\dagger Z^\dagger Z^\dagger Z^\dagger]$	0.026 +i0.026	-0.011 -i0.005	-0.043 -i0.052	-0.003 -i0.015
$[Z^\dagger Z^\dagger Z^\dagger Z^\dagger Z^\dagger]$	-0.003 +i0.001	0.004 +i0.008	0.003 -i0.033	-0.017 -i0.060
Charge	$l = 3$	$l = -3$	$l = 1$	$l = -1$

Table 12: Assignment of charges ± 3 and ± 1 to the 6-9 states.

The procedure should by now be clear, and we present the assignment of non-zero charges to the states 10-13 in table 13. Again, components vanish to within less than 5%, except for those set to 1, and the 2-particle components $\bar{v}_{[ZZ]}^{12}$ and $\bar{v}_{[Z^\dagger Z^\dagger]}^{13}$, also with $l = \pm 2$ charges. Interestingly, as that need not be the case, the $l = 0$ states are also degenerate. A summary of the charge assignments of the states e_{3-15} is presented in table 14.

The approach can be extended for higher states, but it is clear that a more efficient and systematic way to do so would be to start directly with two complex matrices. This is under current investigation, but beyond the scope of this communication.

3.2.3 Massless excitations

We now turn our attention to the lowest excited states e_1 and e_2 . Numerically, their masses do not increase with the coupling, and remain very small compared with the other massive excited states. These are the $U(N)$ traced constituent single particle states $\text{Tr}X_1$ and $\text{Tr}X_2$, and we associate them with the non interacting (free) $U(1) \times U(1)$ subgroup of (8). Numerically, one should be reminded that the eigenvalues of the mass matrix (7) include $N_{\text{loops}} - N_\Omega$ unphysical zero eigenvalues, so these modes will mix with physical zero modes if present in the system. In order to confirm numerically that, indeed, our interpretation that e_1 and e_2 are decoupled zero mass states, we "switch on" masses in the Hamiltonian and seek evidence that indeed e_1 and e_2 remain decoupled states with masses equal to their "bare" masses. This will also allow us to compare our results with the few planar results available in the literature. This is carried out in the next section.

	Doublet		Doublet	
	\bar{v}^{10}	\bar{v}^{11}	\bar{v}^{12}	\bar{v}^{13}
[ZZ]	0.008+i0.004	0.005-i0.002	-0.472+i0.007	-0.016+i0.006
[ZZ†]	-0.005+i0.000	-0.005-i0.000	0.043+i0.020	0.0430-i0.020
[Z†Z†]	0.005+i0.002	0.008-i0.004	-0.016-i0.006	-0.472-i0.007
[Z ³]	-0.004+i0.004	-0.000-i0.000	0.004-i0.018	0.009-i0.002
[ZZZ†]	-0.046+i0.079	0.043-i0.004	-0.000+i0.001	-0.009+i0.012
[ZZ†Z†]	0.043+i0.004	-0.046-i0.079	-0.009-i0.012	-0.000-i0.001
[Z†Z†Z†]	-0.000+i0.000	-0.004-i0.004	0.009+i0.002	0.004+i0.018
[ZZZZ]	1.000+i0.000	-0.000+i0.000	0.021-i0.013	-0.033+i0.009
[ZZZZ†]	-0.025-i0.002	-0.021+i0.027	1.000+i0.000	-0.000+i0.000
[ZZZ†Z†]	0.008+i0.005	0.008-i0.005	-0.041-i0.030	-0.041+i0.030
[ZZ†ZZ†]	0.002+i0.001	0.002-i0.001	-0.023-i0.009	-0.023+i0.009
[ZZ†Z†Z†]	-0.021-i0.027	-0.025+i0.002	0.000+i0.000	1.000+i0.000
[Z†Z†Z†Z†]	-0.000+i0.000	1.000-i0.000	-0.033-i0.009	0.021+i0.013
Charge	$l = 4$	$l = -4$	$l = 2$	$l = -2$

Table 13: Assignment of charges ± 4 and ± 2 to the 10-15 states.

	Degeneracy	Charge
$e_{3,4}$	doublet	$l = \pm 2$
e_5	singlet	$l = 0$
$e_{6,7}$	doublet	$l = \pm 3$
$e_{8,9}$	doublet	$l = \pm 1$
$e_{10,11}$	doublet	$l = \pm 4$
$e_{12,13}$	doublet	$l = \pm 2$
$e_{14,15}$	doublet	$l = 0$

Table 14: Assignment of charges and degeneracies to the 3-15 states..

4 Yang-Mills coupled Hamiltonian with mass

In this section, we consider the matrix quantum mechanical Hamiltonian

$$\hat{H} = \frac{1}{2} \sum_{A=1}^2 \text{Tr} P_A^2 + \frac{m^2}{2} \sum_{A=1}^2 \text{Tr} X_A^2 - \frac{g_{YM}^2}{N} \text{Tr} [X_1, X_2]^2. \quad (12)$$

The same loop truncation with 2615 loops ($l_{\max} = 14$) and Ω a 93×93 matrix is used. We fix $m = 2$ and take $g_{YM} = 0, 1, \dots, 15$. Numerical results for the planar large N energy, the planar even loop correlator values, the planar $l = 0$ complex matrices loop correlator values,¹⁹ and the first 15 mass spectra are displayed in table 15.

¹⁹The loop correlators with an odd number of any of the hermitian matrices are numerically 0 to 4 decimal places with very few exceptions, where their values do not exceed 3×10^{-4} , and similarly for complex matrices loop correlators with non-zero $U(1)$ charges. As such, they are not displayed.

$g_V M$	0	1	2	3	4	5	6	7	8	9	10	11	12	13	14	15
e_0/N^2	2.00000	2.10908	2.34396	2.61780	2.90090	3.18318	3.46097	3.73293	3.99883	4.25863	4.51261	4.76107	5.00439	5.24285	5.47664	5.70642
$\text{Tr} 1/N$	1.0000	1.0000	1.0000	1.0000	1.0000	1.0000	1.0000	1.0000	1.0000	1.0000	1.0000	1.0000	1.0000	1.0000	1.0000	1.0000
$[11]/N^2$	0.2500	0.2273	0.1946	0.1691	0.1499	0.1350	0.1232	0.1137	0.1057	0.0989	0.0931	0.0881	0.0837	0.0798	0.0763	0.0731
$[22]/N^2$	0.2500	0.2273	0.1946	0.1691	0.1499	0.1350	0.1232	0.1136	0.1057	0.0989	0.0931	0.0881	0.0837	0.0798	0.0763	0.0731
$[ZZ]/N^2$	0.5000	0.4546	0.3892	0.3382	0.2998	0.2700	0.2464	0.2273	0.2114	0.1978	0.1862	0.1762	0.1674	0.1596	0.1526	0.1462
$[111]/N^3$	0.1250	0.1034	0.0759	0.0574	0.0451	0.0367	0.0305	0.0260	0.0225	0.0197	0.0175	0.0156	0.0141	0.0128	0.0117	0.0108
$[1122]/N^3$	0.0625	0.0506	0.0362	0.0269	0.0210	0.0169	0.0140	0.0119	0.0102	0.0089	0.0079	0.0071	0.0064	0.0058	0.0053	0.0049
$[1212]/N^3$	0.0000	0.0021	0.0035	0.0035	0.0032	0.0029	0.0025	0.0023	0.0020	0.0018	0.0016	0.0015	0.0014	0.0012	0.0012	0.0011
$[2222]/N^3$	0.1250	0.1034	0.0759	0.0574	0.0451	0.0367	0.0306	0.0260	0.0225	0.0197	0.0175	0.0156	0.0141	0.0128	0.0117	0.0108
$[ZZ^1ZZ^1]/N^3$	0.2750	0.4050	0.2896	0.2154	0.1678	0.1352	0.1121	0.0950	0.0818	0.0714	0.0634	0.0566	0.0510	0.0464	0.0422	0.0390
$[ZZZ^1Z^1]/N^3$	0.2500	0.2110	0.1588	0.1218	0.0966	0.0792	0.0661	0.0566	0.0490	0.0430	0.0382	0.0342	0.031	0.0280	0.0258	0.0238
e_1	2.0000	2.0000	1.9995	1.9980	1.9954	1.9919	1.9887	1.9805	1.9798	1.9722	1.9674	1.9596	1.9536	1.9471	1.9279	1.9334
e_2	2.0000	2.0000	1.9995	1.9981	1.9957	1.9925	1.9890	1.9819	1.9805	1.9728	1.9701	1.9606	1.9558	1.9483	1.9315	1.9384
e_3	4.0000	4.2078	4.6242	5.0937	5.5751	6.0549	6.5295	6.9938	7.4520	7.8999	8.3399	8.7703	9.1924	9.6087	10.011	10.418
e_4	4.0000	4.2080	4.6242	5.0937	5.5753	6.0556	6.5298	6.9946	7.4529	7.9006	8.3405	8.7714	9.1933	9.6094	10.013	10.419
e_5	4.0000	4.5327	5.0772	5.5688	6.1573	6.7943	7.4861	8.0037	8.3936	8.9599	9.3389	9.8451	10.363	10.900	11.237	11.649
e_6	5.5051	6.0541	6.9025	7.5558	8.3571	9.0595	9.5955	10.231	11.104	11.752	12.151	13.057	13.534	14.293	14.483	15.378
e_7	5.9371	6.2794	6.9162	7.6186	8.3691	9.1177	9.8334	10.444	11.232	11.829	12.646	13.131	13.799	14.457	14.694	15.627
e_8	5.9609	6.4296	7.1186	8.2597	9.6060	10.762	11.366	12.184	13.181	13.928	14.740	15.624	15.891	17.179	17.700	18.508
e_9	5.9697	6.6118	7.6290	8.5949	9.8060	10.813	11.689	12.631	13.481	14.259	14.929	15.947	16.264	17.518	18.175	18.801
e_{10}	7.8321	8.3047	7.7023	8.7651	9.8374	11.085	11.888	13.652	14.408	15.339	15.973	17.212	18.158	19.068	19.312	20.362
e_{11}	7.8697	8.3887	9.1365	10.070	11.048	12.009	12.887	13.755	14.822	15.683	16.549	17.424	18.188	19.166	19.669	20.739
e_{12}	7.8841	8.5108	9.1522	10.076	11.100	12.021	12.955	14.199	14.831	15.822	16.703	17.456	18.381	19.388	19.836	20.828
e_{13}	7.9591	8.6885	9.8906	11.191	12.628	13.785	14.886	15.669	17.344	18.062	18.980	20.684	21.265	22.673	22.521	24.244
e_{14}	7.9652	8.7147	9.9857	11.353	12.656	13.907	15.093	16.102	17.492	18.516	19.618	20.859	21.667	22.943	22.705	24.927
e_{15}	7.9911	9.5729	10.056	11.655	13.323	14.743	15.942	16.575	18.284	19.388	20.456	21.426	21.988	23.350	23.117	25.383

Table 15: Numerical results obtained with a truncation to 2615 loops ($l_{\max} = 14$) with Ω a 93×93 matrix with $m = 2$.

4.1 Planar limit

Given that the leading large g_{YM} behaviour of the large N energy, that of the massless limit, has been established in the previous section, we carry out a logarithmic fit of $e_0/N^2 - 0.8890 g_{YM}^{2/3}$ to $b g_{YM}^p$ for large g_{YM} to obtain the next, mass dependent, power dependence on g_{YM} . The logarithmic fit is shown in Figure 9 for $g_{YM} \geq 10$. The least squares fit result for the exponent is $-0.630(2)$, in other words $p = -2/3$ to a high degree of accuracy. Setting $p = -2/3$, we obtain at this truncation level:

$$e_0/N^2 = 0.8890(2) \lambda^{1/3} + 1.807(4) \lambda^{-1/3} + \dots$$

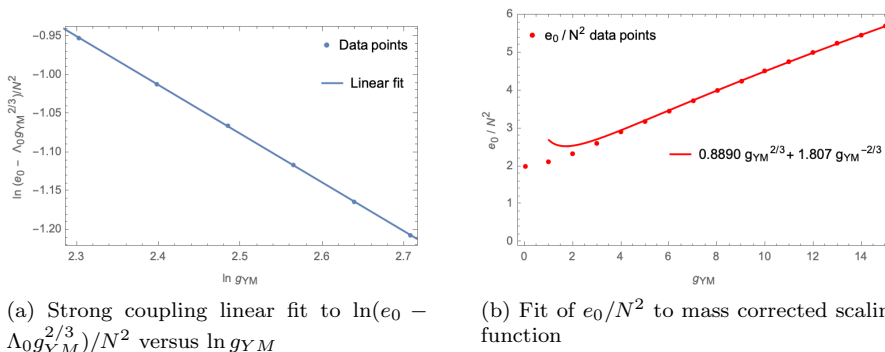


Figure 9: Numerically obtained large N ground state energies and fit to mass corrected scaling function

Since $m = 2$, one has

$$e_0/N^2 = 0.8890(2) \lambda^{1/3} + 0.4518(1) \frac{m^2}{\lambda^{1/3}} + \dots$$

For $\ln \text{Tr} Z^\dagger Z/N^2$, $\text{Tr}(Z^\dagger Z Z^\dagger Z)/N^3$ and $\text{Tr}(Z^\dagger Z^\dagger Z Z)/N^3$ large N correlators, we limit ourselves in displaying the large g_{YM} scaling asymptotes. These are shown in Figure 10

Table 16 compares our large N planar results to those available in the literature. For the large N ground state energy, the improved accuracy of our ap-

	This article	[23]	[42]
e_0/N^2	$0.8890(2) \lambda^{1/3} + 0.4518(1) \frac{m^2}{\lambda^{1/3}} + \dots$	$0.882 \lambda^{1/3} + \dots$	$0.882 \lambda^{1/3} + 0.401 \frac{m^2}{\lambda^{1/3}} + \dots$
$\text{Tr} Z^\dagger Z/N^2$	$0.930(1) \lambda^{-1/3} + \dots$	$0.913 \lambda^{-1/3} + \dots$	$0.968 \lambda^{-1/3} + \dots$

Table 16: Literature comparison

proach is apparent. We also expect the leading g_{YM} dependence for $\text{Tr} Z^\dagger Z/N^2$ to be the most accurate, as we are able to obtain it directly in the massless limit, whereas, as is evident from Figure 10, it may be difficult to extrapolate the leading dependence on g_{YM} from the strong coupling regime of an Hamiltonian with mass, as is the case in [42], [23].

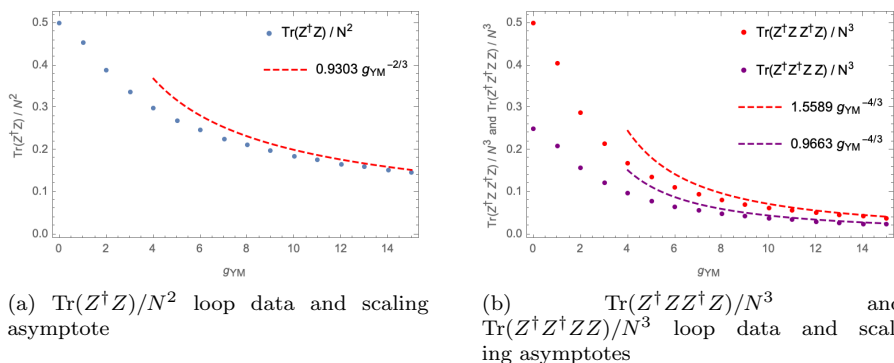
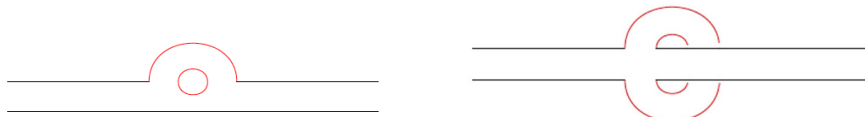


Figure 10: Numerically obtained large N loops with two and four matrices and their scaling asymptotes

4.2 $1/N$ spectrum

Inspection of table 15 shows that the energies e_1 and e_2 remain constant and very close to the "bare" mass value $m = 2^{20}$. In the massless limit then, these states remain massless, confirming the interpretation provided in the previous section.

This may be surprising from a diagrammatic point of view. Indeed, as an example, to order $\lambda = g_{YM}^2$, one has the usual planar and non-planar contribution to the connected 2-point function $\langle X_1(t_2)_{a_1 a_2} X_1(t_1)_{b_1 b_2} \rangle / N^3$, as shown in Figure 11.



(a) The planar 2 point vertex function is:

$$-\frac{2i\lambda}{mN^3} \delta_{a_1 b_2} \delta_{a_2 b_1} .$$

(b) Non-planar 2 point vertex function is

$$\frac{2i\lambda}{mN^4} \delta_{a_1 a_2} \delta_{b_2 b_1} .$$

Figure 11: Order $\lambda = g_{YM}^2$ diagrams contributing to the 2 point vertex function of $\langle X_1(t_2)_{a_1 a_2} X_1(t_1)_{b_1 b_2} \rangle / N^3$. Note the difference in the structure of the index contractions.

However, when the external legs are contracted, we see that the two diagrams of the previous figure cancel out, as shown in Figure 12

To the same order, one can also show diagrammatically, for instance, the decoupling of 1-particle to 3-particle states²¹.

These are, however, simple perturbative results, but numerically it is established that, non-perturbatively, the states do not receive (finite) corrections to

²⁰The slight decrease with g_{YM} is attributed to the fact that, numerically, the unphysical "zero modes" develop small finite values. This is in opposition to the case of a quartic potential [44], and seemingly characteristic of a Yang-Mills potential in the context of our approach

²¹Namely, the connected contribution to $\langle \text{Tr}(X_1 X_2^2)(t_2) \text{Tr} X_1(t_1) \rangle$

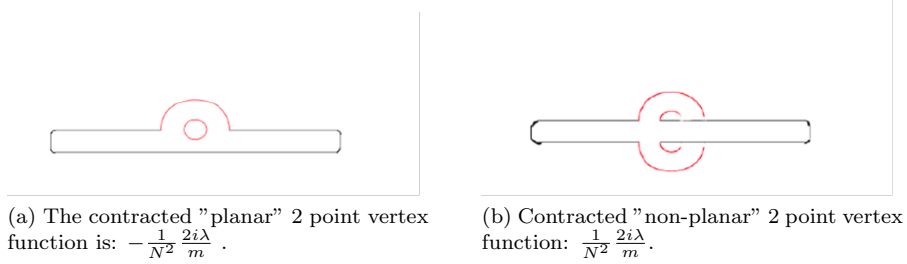


Figure 12: Order $\lambda = g_{YM}^2$ cancellation of contracted diagrams contributing to the 2 point vertex function of $\langle \text{Tr}X_1(t_2)\text{Tr}X_1(t_1) \rangle / N^3$.

the "bare" mass and decouple from higher (bound) states.

Finally, for the states with energies $e_{3,4,5}$, we proceed as for e_0/N^2 to obtain the following mass corrected scaling functions:

$$\begin{aligned} e_1 &= 1.588(1)\lambda^{1/3} + 4.57(2)\lambda^{-1/3} + \dots \\ e_2 &= 1.588(1)\lambda^{1/3} + 4.56(2)\lambda^{-1/3} + \dots \\ e_3 &= 1.862(8)\lambda^{1/3} + 2.9(2)\lambda^{-1/3} + \dots \end{aligned}$$

or,

$$\begin{aligned} e_1 &= 1.588(1)\lambda^{1/3} + 1.14(1)\frac{m^2}{\lambda^{1/3}} + \dots \\ e_2 &= 1.588(1)\lambda^{1/3} + 1.14(1)\frac{m^2}{\lambda^{1/3}} + \dots \\ e_3 &= 1.862(8)\lambda^{1/3} + 0.73(1)\frac{m^2}{\lambda^{1/3}} + \dots \end{aligned}$$

The above mass corrected scaling functions are displayed together with the numerically obtained energies in Figure 13. The agreement for the two lowest lying degenerate bound states at large g_{YM} is excellent.

There are no spectrum results available in the literature for comparison, as far as we know.

The assignment of charges is carried out in the same way as in the massless case, for $m = 2$ and $g_{YM} = 10$, and for a $l_{\max} = 10$ mass spectrum subsector on the full $l_{\max} = 14$ planar background. They are summarised in table 17²².

5 Discussion and outlook

We studied the large N dynamics of two massless Yang-Mills coupled matrix quantum mechanics, by minimization of a loop truncated Jevicki-Sakita effective collective field Hamiltonian. The loop space constraints are handled by the use of master variables.

The method was successfully applied directly in the massless limit for a range of values of the Yang-Mills coupling constant, and the scaling behaviour

²²The e_{12} mass displays an irregular behaviour across the range of coupling constants, as was the case in the massless system.

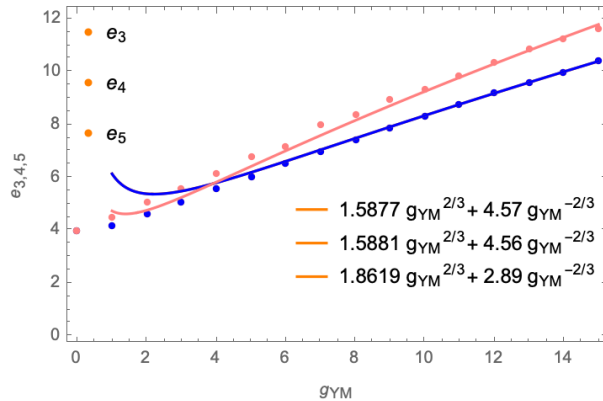


Figure 13: Numerical results for the masses $e_{3,4,5}$ and fit to mass corrected scaling functions

n	e_n	Charge
e_3	8.34(1)	$l = \pm 2$
e_4	8.34(1)	
e_5	9.3(4)	$l = 0$
e_6	12.2(2)	$l = \pm 3$
e_7	12.6(5)	
e_8	15(1)	$l = \pm 1$
e_9	15(1)	
e_{10}	16.0(8)	$l = \pm 4$
e_{11}	16.5(2)	
e_{12}	16.7(1)	$l = \pm 2$
e_{13}	19.0(2)	
e_{14}	19.6(1)	$l = 0$
e_{15}	20.5(9)	

Table 17: Assignment of charges to states 3-15 for $m = 2$ at $g_{YM} = 10$

of different physical quantities derived from their dimensions were obtained with a high level of precision. Planar correlators of non-zero charge were shown to vanish to a high degree of accuracy, and the expected charged spectrum degeneracies confirmed for a high number of states. This attests to the validity of the method, to the consistency of the truncation scheme and to the use of master variables.

We considered both planar properties of the theory, such as the large N ground state energy and multi-matrix correlator expectation values, and also the $1/N$ spectrum of the theory.

For the spectrum, we established that the $U(N)$ traced fundamental constituents remain massless and decoupled from other states, and that bound states develop well defined mass gaps, with the mass of the two degenerate lowest lying bound states being determined with a particularly high degree of accuracy. These results clarify whether the system has or does not have a mass gap, and establish the nature of its patterns.

As, potentially, the presence of massless states in the spectrum may present challenges in their identification, given the nature of the numerical scheme used, we also considered the case where the fundamental constituents have a finite "bare mass", and confirmed that their $U(N)$ traced masses do not receive radiative corrections, and that they decouple from the remaining bound states in the spectrum. This also allowed us to compare some planar results with the small number of results available in the literature. As we are able to obtain the asymptotic large λ behaviour of different physical quantities directly in the massless limit, we expect our results to be more accurate for planar quantities, and new, for the $1/N$ spectrum with finite "bare masses" as well.

Generalization to 3 matrices, currently under investigation, is of clear physical interest, as is the possibility of adding large N quenching to the master field construction. On the "string/gravity" side, despite the absence of fermionic degrees of freedom and of a chiral limit, it is an interesting question to investigate if a BMN-type spectrum is present [52],[53],[54],[55],[56],[57] and other dual gravity properties. In this regard, the application of the method described in this article directly to complex matrices and chiral states is of interest, and currently under investigation. The addition of fermionic degrees of freedom and, more broadly, the generalization to supersymmetric systems is, of course, of great interest.

6 Appendix A - Effects of truncation parameters

In any numerical scheme involving a truncated system, it is important to try and estimate errors associated with the truncation itself, and with the different parameters of the algorithm. The accuracy of the numerical results presented in this article depend on three parameters: the truncation level l (and corresponding l_{\max}), N (for a given l) and the convergence criterium of the optimization. We first discuss the loop truncation.

6.1 Loop truncation

The results presented in the main body of this article were obtained with $l = 8$, corresponding to a loop truncation involving the 2615 single trace operators with length less or equal to $l_{\max} = 14$, and 2652 master variables ($N = 51$). Ω is a 93×93 matrix. For a few values of g_{YM} , we ran the optimization code for $l = 9$, corresponding to a loop truncation involving the 8923 single trace operators with length less or equal to $l_{\max} = 16$, and 8930 master variables ($N = 94$). In this case, Ω is a 153×153 matrix. A number of planar quantities are displayed in tables 18 and 19 for $g_{YM} = 6, 8, 10$, for both the massless case (18) and for mass $m = 2$ (19).

The first observation is how accurate ($\sim 0.02\% - 0.04\%$) the ground state energy is with respect to truncation dependence. For loops up to quartic loops, in general the accuracy is less than 0.3%, except for a single loop where one can expect a truncation effect of $\sim 0.9\%$. This is incorporated in the body of the article, where we have followed a very conservative approach and in general used the least accurate estimate.

	$g_{YM} = 6$			$g_{YM} = 8$			$g_{YM} = 10$		
	$l_{\max} = 14$	$l_{\max} = 16$	% diff.	$l_{\max} = 14$	$l_{\max} = 16$	% diff.	$l_{\max} = 14$	$l_{\max} = 16$	% diff.
e_0/N^2	2.9355	2.9343	0.04%	3.5562	3.5547	0.04%	4.1266	4.1249	0.04%
Tr $1/N$	1.0000	1.0000	fixed	1.0000	1.0000	fixed	1.0000	1.0000	fixed
$[11]/N^2$	0.1409	0.1411	-0.15 %	0.1163	0.1164	-0.17 %	0.1002	0.1004	-0.16%
$[22]/N^2$	0.1409	0.1411	-0.16 %	0.1163	0.1164	-0.16 %	0.1002	0.1004	-0.16%
$[1111]/N^3$	0.0400	0.0401	-0.26%	0.0273	0.0273	-0.28 %	0.0203	0.0203	-0.26%
$[1122]/N^3$	0.0179	0.0179	-0.18%	0.0122	0.0122	-0.19%	0.0090	0.0091	-0.20%
$[1212]/N^3$	0.0043	0.0043	-0.90%	0.0029	0.0029	-0.92%	0.0022	0.0022	-0.98%
$[2222]/N^3$	0.0400	0.0401	-0.27%	0.0273	0.0273	-0.27%	0.0202	0.0203	-0.27%

Table 18: Loop truncation dependence of planar large N energy and expectation values of single trace operators - massless case

	$g_{YM} = 6$			$g_{YM} = 8$			$g_{YM} = 10$		
	$l_{\max} = 14$	$l_{\max} = 16$	% diff.	$l_{\max} = 14$	$l_{\max} = 16$	% diff.	$l_{\max} = 14$	$l_{\max} = 16$	% diff.
e_0/N^2	3.4610	3.4604	0.02%	3.9988	3.9979	0.02%	4.5126	4.5114	0.03%
Tr $1/N$	1.0000	1.0000	fixed	1.0000	1.0000	fixed	1.0000	1.0000	fixed
$[11]/N^2$	0.1232	0.1233	-0.07%	0.1057	0.1058	-0.10%	0.0931	0.0932	-0.11%
$[22]/N^2$	0.1232	0.1233	-0.07%	0.1057	0.1058	-0.10%	0.0931	0.0932	-0.12%
$[1111]/N^3$	0.0305	0.0306	-0.11%	0.0225	0.0225	-0.16%	0.0175	0.0175	-0.18%
$[1122]/N^3$	0.0140	0.0140	-0.06%	0.0102	0.0102	-0.10%	0.0079	0.0079	-0.12%
$[1212]/N^3$	0.0025	0.0026	-0.57%	0.0020	0.0020	-0.74%	0.0016	0.0016	-0.81%
$[2222]/N^3$	0.0306	0.0306	-0.11%	0.0225	0.0225	-0.16%	0.0175	0.0175	-0.19%

Table 19: Loop truncation dependence of planar large N energy and expectation values of single trace operators with mass $m = 2$

Tables 20 and 21 present similar results for the bound states e_3 to e_{15} . We observe the accuracy of the two degenerate lowest lying bound states ($e_{4,5}$) and their insensitivity to truncation to within ($\sim 0.07\% - 0.13\%$). For higher states, the effects of the truncation vary from state to state, but except for $g_{YM} = 6$ in the massless case, they are found to be at most 5 – 6%, with many states much less. The case of $g_{YM} = 6$ in the massless case displays larger truncation effects. Although requiring further understanding, these are the values used in the main body of the article, in line with our conservative approach to error estimation.

	$g_{YM} = 6$			$g_{YM} = 8$			$g_{YM} = 10$		
	$l_{\max} = 14$	$l_{\max} = 16$	% diff.	$l_{\max} = 14$	$l_{\max} = 16$	% diff.	$l_{\max} = 14$	$l_{\max} = 16$	% diff.
e_3	5.2431	5.2368	0.12%	6.3508	6.3436	0.11%	7.3699	7.3605	0.13%
e_4	5.2446	5.2384	0.12%	6.3524	6.3449	0.12%	7.3721	7.3621	0.14%
e_5	6.1860	5.9766	3.39%	7.2823	7.0897	2.64%	8.4041	8.2057	2.36%
e_6	7.8667	7.6625	2.60%	9.4180	9.2940	1.32%	10.863	10.803	0.55%
e_7	8.0208	7.8264	2.42%	9.5160	9.4329	0.87%	11.175	10.861	2.81%
e_8	9.7959	9.0238	7.88%	11.338	11.035	2.66%	13.163	12.603	4.25%
e_9	9.9158	9.2379	6.84%	11.717	11.099	5.27%	13.324	12.969	2.66%
e_{10}	10.538	10.437	0.96%	12.661	12.590	0.56%	14.655	14.558	0.66%
e_{11}	10.605	10.466	1.31%	12.732	12.700	0.25%	14.763	14.617	0.99%
e_{12}	12.174	10.946	10.1%	13.181	12.785	3.01%	15.327	14.786	3.53%
e_{13}	12.494	12.303	1.53%	15.133	14.682	2.98%	17.465	17.019	2.56%
e_{14}	12.813	12.367	3.49%	15.233	15.107	0.82%	17.776	17.460	1.78%
e_{15}	13.202	12.689	3.88%	15.558	15.349	1.34%	18.020	17.683	1.87%

Table 20: Loop truncation dependence of spectrum - massless limit

The parameter $gtol$ provides a convergence criterium for the optimization

	$g_{YM} = 6$			$g_{YM} = 8$			$g_{YM} = 10$		
	$l_{\max} = 14$	$l_{\max} = 16$	% diff.	$l_{\max} = 14$	$l_{\max} = 16$	% diff.	$l_{\max} = 14$	$l_{\max} = 16$	% diff.
e_3	6.5295	6.5252	0.07%	7.4520	7.4459	0.08%	8.3399	8.3317	0.10%
e_4	6.5298	6.5255	0.07%	7.4529	7.4465	0.09%	8.3405	8.3328	0.09%
e_5	7.1861	7.0791	1.49%	8.3936	7.8712	6.22%	9.3389	8.9426	4.24%
e_6	9.5955	9.5390	0.59%	11.104	10.704	3.60%	12.151	11.991	1.32%
e_7	9.8334	9.5793	2.58%	11.232	10.802	3.83%	12.646	12.119	4.17%
e_8	11.367	10.779	5.17%	13.181	12.046	8.61%	14.740	13.731	6.85%
e_9	11.689	10.934	6.46%	13.481	12.239	9.21%	14.929	13.819	7.44%
e_{10}	11.888	11.536	2.96%	14.409	13.142	8.79%	15.973	15.189	4.91%
e_{11}	12.887	12.985	-0.76%	14.822	14.674	1.00%	16.549	16.390	0.96%
e_{12}	12.955	13.002	-0.36%	14.831	14.809	0.15%	16.703	16.566	0.82%
e_{13}	14.886	15.168	-1.89%	17.344	16.794	3.17%	18.980	18.739	1.27%
e_{14}	15.094	15.273	-1.19%	17.493	17.405	0.50%	19.618	19.510	0.55%
e_{15}	15.942	15.591	2.20%	18.284	17.471	4.45%	20.456	19.598	4.19%

Table 21: Loop truncation dependence of spectrum - $mass = 2$

program, being the maximum norm of the gradient vector at the minimum. Tables 22 and 23 compare planar and spectral data obtained with an average gradient component of 10^{-08} (the criterium used to obtain the results in the body of the article) versus 10^{-09} . It is seen that they are consistently less than loop truncation effects.

	$g_{YM} = 6$			$g_{YM} = 12$		
	10^{-08}	10^{-09}	% diff.	10^{-08}	10^{-09}	% diff.
$gtol/\sqrt{N(N+1)}$						
e_0/N^2	2.9355	2.9355	0.00%	4.6600	4.6600	0.00%
$\text{Tr } 1/N$	1.0000	1.0000	fixed	1.0000	1.0000	fixed
$[11]/N^2$	0.1409	0.1409	-0.01%	0.0887	0.0887	0.00%
$[22]/N^2$	0.1409	0.1409	0.00%	0.0887	0.0887	0.00%
$[1111]/N^3$	0.0400	0.0400	-0.01%	0.0159	0.0159	0.00%
$[1122]/N^3$	0.0179	0.0179	0.00%	0.0071	0.0071	0.00%
$[1212]/N^3$	0.0043	0.0179	-0.02%	0.0017	0.0017	0.00%
$[2222]/N^3$	0.0400	0.0400	-0.02%	0.0159	0.0159	0.00%

Table 22: gtol dependence of planar large N energy and expectation values of single trace operators - massless case

Finally, table 24 compares planar and spectrum results for $N = 51$ (2652 master variables) with those obtained with $N = 52$ (2756 master variables). Once again it is seen that the changes are consistently less than loop truncation effects.

7 Acknowledgments

We thank Robert de Mello Koch for comments on an earlier draft of this article and Antal Jevicki for his encouragement to continue to work on loop space based numerical schemes. One of us (JPR) thanks him for his hospitality during a recent visit to the Brown Theoretical Physics Center, where the latest version of the article was completed. We also thank Xialong (Shannon) Liu for fruitful discussions. This work is supported by the National Institute for Theoretical and Computational Sciences, NRF Grant Number 65212.

$gtol/\sqrt{N(N+1)}$	$g_{YM} = 6$			$g_{YM} = 12$		
	10^{-08}	10^{-09}	% diff.	10^{-08}	10^{-09}	% diff.
e_3	5.2431	5.2444	-0.02%	8.3206	8.3203	0.00%
e_4	5.2446	5.2446	0.00%	8.3206	8.3203	0.00%
e_5	6.1860	6.1540	0.52%	9.5306	9.5364	-0.06%
e_6	7.8667	7.7556	1.41%	12.341	12.361	-0.17%
e_7	8.0208	7.9610	1.41%	12.574	12.577	-0.03%
e_8	9.7959	9.5779	2.23%	14.850	14.891	-0.27%
e_9	9.9158	9.5779	1.69%	15.107	15.147	-0.27%
e_{10}	10.538	9.7479	1.85%	16.529	16.542	-0.07%
e_{11}	10.605	10.533	0.68%	16.576	16.579	-0.02%
e_{12}	12.174	12.126	0.39%	17.522	17.543	-0.12%
e_{13}	12.494	12.361	1.07%	17.522	17.543	-0.12%
e_{14}	12.813	12.574	1.87%	19.990	20.025	-0.17%
e_{15}	13.202	12.574	1.26%	20.128	20.151	-0.11%

Table 23: $gtol$ dependence of spectrum - massless limit

	$g_{YM} = 6$		
	$N = 51$	$N = 52$	% diff.
e_0/N^2	3.4610	3.4609	0.00%
Tr $1/N$	1.0000	1.0000	fixed
$[11]/N^2$	0.1232	0.1233	-0.01%
$[22]/N^2$	0.1232	0.1233	-0.01%
$[1111]/N^3$	0.0305	0.0306	-0.03%
$[1122]/N^3$	0.0140	0.0140	-0.02%
$[1212]/N^3$	0.0020	0.0020	-0.74%
$[2222]/N^3$	0.0025	0.0025	-0.13%
e_3	6.5295	6.5287	0.01%
e_4	6.5298	6.5290	0.01%
e_5	7.1861	7.3927	-2.88%
e_6	9.5955	9.7150	-1.25%
e_7	9.8334	9.7692	0.65%
e_8	11.367	11.498	-1.16%
e_9	11.689	11.740	-0.44%
e_{10}	11.888	12.700	-6.83%
e_{11}	12.887	12.914	-0.21%
e_{12}	12.955	12.977	-0.17%
e_{13}	14.886	15.002	-0.78%
e_{14}	15.094	15.119	-0.17%
e_{15}	15.942	15.855	0.54%

Table 24: N dependence

References

- [1] G. 't Hooft, Nucl. Phys. B **72**, 461 (1974) doi:10.1016/0550-3213(74)90154-0
- [2] T. Eguchi and H. Kawai, Phys. Rev. Lett. **48**, 1063 (1982) doi:10.1103/PhysRevLett.48.1063
- [3] G. Bhanot, U. M. Heller and H. Neuberger, Phys. Lett. B **113**, 47-50 (1982) doi:10.1016/0370-2693(82)90106-X

- [4] G. Parisi, Phys. Lett. B **112**, 463-464 (1982) doi:10.1016/0370-2693(82)90849-8
- [5] D. J. Gross and Y. Kitazawa, Nucl. Phys. B **206**, 440-472 (1982) doi:10.1016/0550-3213(82)90278-4
- [6] S. R. Das and S. R. Wadia, Phys. Lett. B **117**, 228 (1982) [erratum: Phys. Lett. B **121**, 456 (1983)] doi:10.1016/0370-2693(82)90552-4
- [7] H. Neuberger, Phys. Lett. B **119**, 179-182 (1982) doi:10.1016/0370-2693(82)90272-6
- [8] Y. Kitazawa and S. R. Wadia, Phys. Lett. B **120**, 377-382 (1983) doi:10.1016/0370-2693(83)90469-0
- [9] J. Polchinski, Phys. Rev. Lett. **75**, 4724-4727 (1995) doi:10.1103/PhysRevLett.75.4724 [arXiv:hep-th/9510017 [hep-th]].
- [10] T. Banks, W. Fischler, S. H. Shenker and L. Susskind, Phys. Rev. D **55**, 5112-5128 (1997) doi:10.1103/PhysRevD.55.5112 [arXiv:hep-th/9610043 [hep-th]].
- [11] N. Ishibashi, H. Kawai, Y. Kitazawa and A. Tsuchiya, Nucl. Phys. B **498**, 467-491 (1997) doi:10.1016/S0550-3213(97)00290-3 [arXiv:hep-th/9612115 [hep-th]].
- [12] J. M. Maldacena, Adv. Theor. Math. Phys. **2**, 231-252 (1998) doi:10.4310/ATMP.1998.v2.n2.a1 [arXiv:hep-th/9711200 [hep-th]].
- [13] S. S. Gubser, I. R. Klebanov and A. M. Polyakov, Phys. Lett. B **428**, 105-114 (1998) doi:10.1016/S0370-2693(98)00377-3 [arXiv:hep-th/9802109 [hep-th]].
- [14] E. Witten, Adv. Theor. Math. Phys. **2**, 253-291 (1998) doi:10.4310/ATMP.1998.v2.n2.a2 [arXiv:hep-th/9802150 [hep-th]].
- [15] N. Beisert, C. Ahn, L. F. Alday, Z. Bajnok, J. M. Drummond, L. Freyhult, N. Gromov, R. A. Janik, V. Kazakov and T. Klose, *et al.* Lett. Math. Phys. **99** (2012), 3-32 doi:10.1007/s11005-011-0529-2 [arXiv:1012.3982 [hep-th]].
- [16] D. E. Berenstein, J. M. Maldacena and H. S. Nastase, JHEP **04**, 013 (2002) doi:10.1088/1126-6708/2002/04/013 [arXiv:hep-th/0202021 [hep-th]].
- [17] R. de Mello Koch, A. Jevicki and J. P. Rodrigues, Int. J. Mod. Phys. A **19** (2004), 1747-1770 doi:10.1142/S0217751X04017847 [arXiv:hep-th/0209155 [hep-th]].
- [18] N. Beisert, C. Kristjansen, J. Plefka and M. Staudacher, Phys. Lett. B **558** (2003), 229-237 doi:10.1016/S0370-2693(03)00269-7 [arXiv:hep-th/0212269 [hep-th]].
- [19] N. Kim, T. Klose and J. Plefka, Nucl. Phys. B **671** (2003), 359-382 doi:10.1016/j.nuclphysb.2003.08.019 [arXiv:hep-th/0306054 [hep-th]].
- [20] V. Kazakov, I. K. Kostov and D. Kutasov, Nucl. Phys. B **622** (2002), 141-188 doi:10.1016/S0550-3213(01)00606-X [arXiv:hep-th/0101011 [hep-th]].

- [21] J. S. Cotler, G. Gur-Ari, M. Hanada, J. Polchinski, P. Saad, S. H. Shenker, D. Stanford, A. Streicher and M. Tezuka, *JHEP* **05** (2017), 118 [erratum: *JHEP* **09** (2018), 002] doi:10.1007/JHEP05(2017)118 [arXiv:1611.04650 [hep-th]].
- [22] J. Maldacena, [arXiv:2303.11534 [hep-th]].
- [23] T. Morita and H. Yoshida, *Phys. Rev. D* **101** (2020) no.10, 106010 doi:10.1103/PhysRevD.101.106010 [arXiv:2001.02109 [hep-th]].
- [24] S. Pateloudis *et al.* [Monte Carlo String/M-theory (MCSMC)], *JHEP* **03** (2023), 071 doi:10.1007/JHEP03(2023)071 [arXiv:2210.04881 [hep-th]].
- [25] B. Simon, *Annals Phys.* **146**, 209-220 (1983) doi:10.1016/0003-4916(83)90057-X
- [26] B. de Wit, J. Hoppe and H. Nicolai, *Nucl. Phys. B* **305**, 545 (1988) doi:10.1016/0550-3213(88)90116-2
- [27] J. Froehlich and J. Hoppe, *Commun. Math. Phys.* **191**, 613-626 (1998) doi:10.1007/s002200050280 [arXiv:hep-th/9701119 [hep-th]].
- [28] A. Jevicki and B. Sakita, *Nucl. Phys. B* **165**, 511 (1980) doi:10.1016/0550-3213(80)90046-2
- [29] S. R. Das and A. Jevicki, *Mod. Phys. Lett. A* **5**, 1639-1650 (1990) doi:10.1142/S0217732390001888
- [30] K. Demeterfi, A. Jevicki and J. P. Rodrigues, *Mod. Phys. Lett. A* **6**, 3199-3212 (1991) doi:10.1142/S0217732391003699
- [31] A. Jevicki, O. Karim, J. P. Rodrigues and H. Levine, *Nucl. Phys. B* **213**, 169-188 (1983) doi:10.1016/0550-3213(83)90180-3
- [32] A. Jevicki, O. Karim, J. P. Rodrigues and H. Levine, *Nucl. Phys. B* **230**, 299-316 (1984) doi:10.1016/0550-3213(84)90215-3
- [33] K. G. Wilson, *Phys. Rev. D* **10**, 2445-2459 (1974) doi:10.1103/PhysRevD.10.2445
- [34] J. P. Rodrigues, *Nucl. Phys. B* **260**, 350-380 (1985) doi:10.1016/0550-3213(85)90077-X
- [35] D. J. Gross and E. Witten, *Phys. Rev. D* **21**, 446-453 (1980) doi:10.1103/PhysRevD.21.446
- [36] A. Jevicki and B. Sakita, *Phys. Rev. D* **22**, 467 (1980) doi:10.1103/PhysRevD.22.467
- [37] S. R. Wadia, *Phys. Lett. B* **93**, 403-410 (1980) doi:10.1016/0370-2693(80)90353-6
- [38] J. P. Rodrigues, *Phys. Rev. D* **26**, 2833 (1982) doi:10.1103/PhysRevD.26.2833

- [39] J. P. Rodrigues, Phys. Rev. D **26**, 2940 (1982) doi:10.1103/PhysRevD.26.2940
- [40] P. D. Anderson and M. Kruczenski, Nucl. Phys. B **921**, 702-726 (2017) doi:10.1016/j.nuclphysb.2017.06.009 [arXiv:1612.08140 [hep-th]].
- [41] H. W. Lin, JHEP **06**, 090 (2020) doi:10.1007/JHEP06(2020)090 [arXiv:2002.08387 [hep-th]].
- [42] X. Han, S. A. Hartnoll and J. Kruthoff, Phys. Rev. Lett. **125**, no.4, 041601 (2020) doi:10.1103/PhysRevLett.125.041601 [arXiv:2004.10212 [hep-th]].
- [43] V. Kazakov and Z. Zheng, JHEP **06**, 030 (2022) doi:10.1007/JHEP06(2022)030 [arXiv:2108.04830 [hep-th]].
- [44] R. d. Koch, A. Jevicki, X. Liu, K. Mathaba and J. P. Rodrigues, JHEP **01**, 168 (2022) doi:10.1007/JHEP01(2022)168 [arXiv:2108.08803 [hep-th]].
- [45] V. Kazakov and Z. Zheng, [arXiv:2203.11360 [hep-th]].
- [46] A. Jevicki and J. P. Rodrigues, Nucl. Phys. B **230**, 317-335 (1984) doi:10.1016/0550-3213(84)90216-5
- [47] D. E. Berenstein, M. Hanada and S. A. Hartnoll, JHEP **02**, 010 (2009) doi:10.1088/1126-6708/2009/02/010 [arXiv:0805.4658 [hep-th]].
- [48] H. Lin, O. Lunin and J. M. Maldacena, JHEP **10**, 025 (2004) doi:10.1088/1126-6708/2004/10/025 [arXiv:hep-th/0409174 [hep-th]].
- [49] E. Marinari and G. Parisi, Phys. Lett. B **240**, 375-380 (1990) doi:10.1016/0370-2693(90)91115-R
- [50] A. Jevicki and J. P. Rodrigues, Phys. Lett. B **268**, 53-58 (1991) doi:10.1016/0370-2693(91)90921-C
- [51] J. P. Rodrigues and A. J. van Tonder, Int. J. Mod. Phys. A **8**, 2517-2550 (1993) doi:10.1142/S0217751X93001004 [arXiv:hep-th/9204061 [hep-th]].
- [52] D. Berenstein, D. H. Correa and S. E. Vazquez, JHEP **02**, 048 (2006) doi:10.1088/1126-6708/2006/02/048 [arXiv:hep-th/0509015 [hep-th]].
- [53] J. P. Rodrigues, JHEP **12**, 043 (2005) doi:10.1088/1126-6708/2005/12/043 [arXiv:hep-th/0510244 [hep-th]].
- [54] R. Bhattacharyya, S. Collins and R. de Mello Koch, JHEP **03**, 044 (2008) doi:10.1088/1126-6708/2008/03/044 [arXiv:0801.2061 [hep-th]].
- [55] D. Berenstein and S. Wang, JHEP **08**, 164 (2022) doi:10.1007/JHEP08(2022)164 [arXiv:2203.15820 [hep-th]].
- [56] S. Pateloudis, G. Bergner, N. Bodendorfer, M. Hanada, E. Rinaldi and A. Schäfer, JHEP **08** (2022), 178 doi:10.1007/JHEP08(2022)178 [arXiv:2205.06098 [hep-th]].
- [57] H. Lin, Nucl. Phys. B **986**, 116066 (2023) doi:10.1016/j.nuclphysb.2022.116066 [arXiv:2206.06524 [hep-th]].